Journal Pre-proof

Graphene quantum dot antioxidant and proautophagic actions protect SH-SY5Y neuroblastoma cells from oxidative stress-mediated apoptotic death

Matija Krunić, Biljana Ristić, Mihajlo Bošnjak, Verica Paunović, Gordana Tovilović-Kovacević, Nevena Zogović, Aleksandar Mirčić, Zoran Marković, Biljana Todorović-Marković, Svetlana Jovanović, Duška Kleut, Miloš Mojović, Đura Nakarada, Olivera Marković, Irena Vuković, Ljubica Harhaji-Trajković, Vladimir Trajković

PII: S0891-5849(21)00776-0

DOI: https://doi.org/10.1016/j.freeradbiomed.2021.10.025

Reference: FRB 15400

To appear in: *Free Radical Biology and Medicine*

Received Date: 10 August 2021

Revised Date: 13 October 2021

Accepted Date: 18 October 2021

Please cite this article as: M. Krunić, B. Ristić, M. Bošnjak, V. Paunović, G. Tovilović-Kovacević, N. Zogović, A. Mirčić, Z. Marković, B. Todorović-Marković, S. Jovanović, Duš. Kleut, Miloš. Mojović, Đ. Nakarada, O. Marković, I. Vuković, L. Harhaji-Trajković, V. Trajković, Graphene quantum dot antioxidant and proautophagic actions protect SH-SY5Y neuroblastoma cells from oxidative stress-mediated apoptotic death, *Free Radical Biology and Medicine* (2021), doi: https://doi.org/10.1016/j.freeradbiomed.2021.10.025.

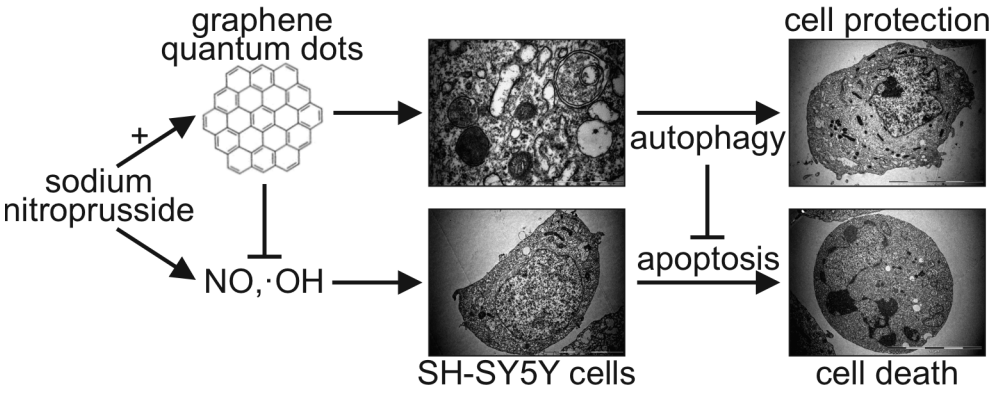

Graphene quantum dot antioxidant and proautophagic actions protect SH-SY5Y neuroblastoma cells from oxidative stress-mediated apoptotic death

Matija Krunić[1#], Biljana Ristić[1#], Mihajlo Bošnjak[1], Verica Paunović[1], Gordana Tovilović-Kovacević[2], Nevena Zogović[3], Aleksandar Mirčić[4], Zoran Marković[5], Biljana Todorović-Marković[5], Svetlana Jovanović[5], Duška Kleut[5], Miloš Mojović[6], Đura Nakarada[6], Olivera Marković[7], Irena Vuković[1], Ljubica Harhaji-Trajković[3]*, Vladimir Trajković[1]*

[1]Institute of Microbiology and Immunology, Faculty of Medicine, University of Belgrade, Dr. Subotića 1, 11000 Belgrade, Serbia

[2]Department of Biochemistry, Institute for Biological Research, "Siniša Stanković"- National Institute of Republic of Serbia, University of Belgrade, Despot Stefan Blvd. 142, 11000 Belgrade, Serbia

[3]Department of Neurophysiology, Institute for Biological Research "Siniša Stanković" - National Institute of Republic of Serbia, University of Belgrade, Despot Stefan Blvd. 142, 11000 Belgrade, Serbia

[4]Institute of Histology and Embryology, Faculty of Medicine, University of Belgrade, Višegradska 26, 11000 Belgrade, Serbia

[5]Vinča Institute of Nuclear Sciences - National Institute of the Republic of Serbia, University of Belgrade P.O. Box 522, 11000 Belgrade, Serbia

[6]Faculty of Physical Chemistry, University of Belgrade, Studentski trg 12-16, 11000 Belgrade, Serbia

[7]Department of Chemistry, Institute of Chemistry, Technology and Metallurgy, University of Belgrade, Njegoševa 12, 11000, Belgrade, Serbia

[#]Equally contributing authors

*Correspondence:
Ljubica Harhaji-Trajković, E-mail: buajk@yahoo.com, Tel: +381113643233, Fax: +381113643235
Vladimir Trajković, E-mail: vladimir.trajkovic@med.bg.ac.rs, Tel: +381113643233, Fax: +381113643235

Abstract

We investigated the ability of graphene quantum dot (GQD) nanoparticles to protect SH-SY5Y human neuroblastoma cells from oxidative/nitrosative stress induced by iron-nitrosyl complex sodium nitroprusside (SNP). GQD reduced SNP cytotoxicity by preventing mitochondrial depolarization, caspase-2 activation, and subsequent apoptotic death. Although GQD diminished the levels of nitric oxide (NO) in SNP-exposed cells, NO scavengers displayed only a slight protective effect, suggesting that NO quenching was not the main protective mechanism of GQD. GQD also reduced SNP-triggered increase in the intracellular levels of hydroxyl radical ($^{\bullet}OH$), superoxide anion ($O_2^{\bullet-}$), and lipid peroxidation. Nonselective antioxidants, $^{\bullet}OH$ scavenging, and iron chelators, but not superoxide dismutase, mimicked GQD cytoprotective activity, indicating that GQD protect cells by neutralizing $^{\bullet}OH$ generated in the presence of SNP-released iron. Cellular internalization of GQD was required for optimal protection, since a removal of extracellular GQD by extensive washing only partly diminished their protective effect. Moreover, GQD cooperated with SNP to induce autophagy, as confirmed by the inhibition of autophagy-limiting Akt/PRAS40/mTOR signaling and increase in autophagy gene transcription, protein levels of proautophagic beclin-1 and LC3-II, formation of autophagic vesicles, and degradation of autophagic target p62. The antioxidant activity of GQD was not involved in autophagy induction, as antioxidants N-acetylcysteine and dimethyl sulfoxide failed to stimulate autophagy in SNP-exposed cells. Pharmacological inhibitors of early (wortmannin, 3-methyladenine) or late stages of autophagy (NH_4Cl) efficiently reduced the protective effect of GQD. Therefore, the ability of GQD to prevent the *in vitro* neurotoxicity of SNP depends on both $^{\bullet}OH$/NO scavenging and induction of cytoprotective autophagy.

Keywords: graphene quantum dots; sodium nitroprusside; neurotoxicity; oxidative stress; hydroxyl radical; nitric oxide; autophagy

Introduction

Excessive amounts of reactive oxygen species (ROS) and reactive nitrogen species (RNS) can cause oxidation and nitration of proteins, lipid peroxidation, DNA damage, ion channel modification, and dissipation of mitochondrial membrane potential, eventually leading to apoptotic or necrotic cell death [1]. The brain is particularly sensitive to oxidative stress due to high consumption of oxygen, high levels of fatty acids susceptible to peroxidation, and a weak antioxidant capacity [2]. ROS and nitric oxide (NO) production by astrocytes and microglia has been implicated in the damage of neuronal and glial cells in Parkinson's disease, Alzheimer's disease, multiple sclerosis and brain ischemia [3,4]. In the reaction with superoxide ($O_2^{\bullet-}$), NO forms peroxynitrite ($ONOO^-$), which further decomposes into highly toxic nitrogen dioxide ($NO_2^{\bullet}$) and hydroxyl radical ($^{\bullet}OH$) [5]. Moreover, $^{\bullet}OH$, $O_2^{\bullet-}$, and hydrogen peroxide (H_2O_2) are generated as by-products of normal cellular respiration and aberrant metabolic processes that utilize molecular oxygen [6]. The complex interactions between oxidative and nitrosative stress in the induction of cell death can be mimicked *in vitro* by sodium nitroprusside (SNP), an iron-nitrosyl complex consisting of a ferrous ion surrounded by five cyanide moieties and a nitrosyl group [7]. In the cell culture, SNP generates both NO and superoxide [8], causing NO- or peroxynitrite-dependent neuronal death [9-12]. Hydroxyl radical produced in the Fenton reaction involving the iron released from SNP has also been found to contribute to its *in vitro* neurotoxicity [13,14].

Antioxidant therapy, although a promising concept based on evidence of oxidative stress involvement in many diseases, including neurodegenerative and neuroinflammatory disorders, largely failed to fulfill the initial expectations. This was mainly due to relatively poor bioavailability, biocompatibility, and antioxidant activity of currently available

compounds [15]. Accordingly, the development of new, more efficient antioxidants has drawn intensive attention in recent years, with graphene quantum dots (GQD) being among the most promising candidates. GQD are up to 100 nm wide, single-to-several layer-thick oval sheets of graphene, a single layer of sp^2-hybridized carbon atoms in a honeycomb structure [16]. They have excellent biocompatibility, broad antioxidant activity superior to that of classic antioxidants, and unique ability to mimic the action of cellular antioxidant enzyme superoxide dismutase [17,18]. The ability of GQD to enter various cell types, including neurons, is well documented [19-23]. While photoactivated GQD generate ROS [21,24-26], in the absence of photoexcitation they act as antioxidants and protect cells by scavenging $^{\bullet}OH$, $O_2^{\bullet-}$ [24,25], and NO [27]. GQD [21,28,29] and SNP [30-32] also induce macroautophagy (hereafter autophagy), a process in which damaged organelles and protein aggregates are sequestered within double-membrane autophagosomes, which subsequently fuse with lysosomes where autophagic cargo is degraded [33]. Autophagy is negatively regulated by Akt/mechanistic target of rapamycin (mTOR) signaling pathway and protects cells from proteotoxic, oxidative, metabolic, and drug-induced stress [33]. Neurons are particularly vulnerable to slowdown in autophagy-dependent proteolytic clearance, and the accumulation of misfolded and damaged proteins in many neurodegenerative diseases is associated with defective autophagy [34,35].

To the best of our knowledge, the effect of GQD on SNP neurotoxicity has not been investigated thus far. Based on the above findings, we hypothesized that GQD might protect neuronal cells from SNP-triggered oxidative/nitrosative stress by acting as both antioxidants and autophagy inducers. Indeed, we here demonstrate for the first time the ability of GQD to prevent apoptotic death of SNP-treated SH-SY5Y neuroblastoma cells by scavenging $^{\bullet}OH$

and to a lesser extent NO, as well as by stimulating cytoprotective autophagy independently of their antioxidant activity.

Material and methods

Synthesis and characterization of GQD

GQD were produced by electrochemical oxidation of graphite rods immersed in 3 mass % of NaOH in ethanol [36]. Synthetic conditions and cleaning phases are described elsewhere [37]. UV/Vis spectra (200 to 800 nm) of GQD sonicated in demineralized water (0.25 mg/mL) were recorded in the air environment at room temperature on GBC Cintra 6 spectrophotometer (GBC, Dandenong, Australia), using quartz cell with 1 cm path length and 4 mL volume. The chemical structure of GQD powder was investigated by Fourier Transform-InfraRed (FTIR) spectroscopy, using Nicolet 6700 FTIR instrument (Thermo Fisher Scientific, Waltham, MA) in attenuated total reflection mode and the spectral resolution set at 2 cm^{-1}. Photoluminescent properties of GQD were investigated using Horiba Jobin Yvon Fluoromax-4 spectrometer (Horiba, Kyoto, Japan). Water dispersion of GQD (0.25 mg/mL) was placed in a quartz cell with a 1 cm path length and 4 mL volume, and the spectra were recorded in the air environment at room temperature, using wavelengths from 300 to 400 nm for the excitation. For the height and lateral size measurement, GQD in demineralized water (0.25 mg/mL) were deposited onto mica substrate by spin coating and investigated by Atomic Force Microscopy (AFM) using a Quesant microscope (Agoura Hills, CA) working in the tapping mode and air environment at 20°C. A Q-WM300 monolithic silicon probe for non-contact high-frequency applications and standard silicon tips (force constant of 40 N/m) (Nano and More Gmbh, Wetzlar, Germany) were used for the imaging, and the open-source Gwyddion software (http://gwyddion.net) was used for the profile

analysis. GQD structure and morphology were additionally analyzed by high-resolution transmission electron microscopy (HR-TEM) using a JEOL JEM-2100F microscope (JEOL, Peabody, MA). Water dispersion of GQD (1 mg/mL) was deposited using drop-casting onto carbon-laced copper grids, and ImageJ software was used to investigate particles in HR-TEM images.

Radical scavenging assays

The general antioxidant capacity of GQD was assessed by measuring their ability to reduce 2,2-diphenyl-1-picrylhydrazyl (DPPH), a purple-colored free stable radical that loses its color when reduced by antioxidants. GQD (50-400 µg/mL) dissolved in TRIS buffer (pH 7.4) were mixed with an equal volume of DPPH (50 µM) in MeOH. After 30 min, the absorbance of the remaining DPPH was measured at 517 nm using a microplate reader, and the results were expressed as the % of control containing only DPPH. The ability of GQD to scavenge Fenton reaction-derived hydroxyl radical was determined by mixing 1 mL of GQD (100 - 400 µg/mL) in PBS with 2 mL of the reaction mixture containing 1 mL of 1.5 mM $FeSO_4$, 0.7 mL of 6 mM H_2O_2, and 0.3 mL of 20 mM sodium salicylate [38]. After 1 h at 37°C, the absorbance of the hydroxylated salicylate complex was measured at 570 nm using a microplate reader. The results were expressed as the % of the control value (without GQD), which was arbitrarily set to 100%. Superoxide anion-scavenging activity of GQD was determined using alkaline DMSO (1 mM NaOH in DMSO) as an $O_2^{\bullet-}$ generating system [39]. The level of $O_2^{\bullet-}$ was assessed by NBT assay, in which NBT reacts with the $O_2^{\bullet-}$ to form a blue NBT-diformazan product. In brief, GQD (100 - 400 µg/mL) were mixed with alkaline DMSO and NBT solution (0.1 mg/mL), and color development was measured at 570 nm using a microplate reader. The results were expressed as the % of the control value (without GQD), which was arbitrarily set to 100%.

Electron paramagnetic resonance (EPR) analysis

For the EPR analysis of GQD quenching activity towards $^{\bullet}OH$, $O_2^{\bullet-}$ and NO radicals, the following well known chemical generators were used: Fenton reaction for $^{\bullet}OH$, riboflavin/light reaction for $O_2^{\bullet-}$, and SNP for NO. All chemicals (analytical grade or higher) were used as received from Merck (Darmstadt, Germany) or Ramidus AB (Lund, Sweden) (for sarcosine-N-dithiocarbamate; DTCS) without any further purification, and spin-trap 5-(Diethoxyphosphoryl)-5-methyl-1-pyrroline-N-oxide (DEPMPO) was purchased from Focus Biomolecules (Plymouth Meeting, PA) and purified as previously described [40]. To detect the quenching activity of GQD towards $^{\bullet}OH$ radicals, the Fenton reaction in the presence of spin-trap DEPMPO was used according to previously developed methodology [41,42]. This spin-trap was chosen because of the good selectivity and a long DEPMPO/OH spin-adduct half-life (132 min) [43]. To avoid the influence of the spin-adduct natural degradation process on the EPR signal, it was important to record EPR spectra immediately after the Fenton reaction was initiated. In brief, 30 µl of sample containing 26 µl of GQD solution (final concentration 0.87 mg/mL), 2 µl of H_2O_2 (final concentration 0.35 mM), 1 µl of DEPMPO (final concentration 3.5 mM) was transferred into the gas-permeable Teflon tube, and 1 µl of $FeSO_4$ (final concentration 0.15 mM) was applied just before the EPR spectra was acquired. Recordings were made using the following experimental settings: microwave power 10 mW, microwave frequency 9.85 GHz, modulation frequency 100 kHz, modulation amplitude 1 G. For the estimation of the $O_2^{\bullet-}$ radical quenching activity of GQD, riboflavin/light generating system was employed [41,42]. 23 µl of GQD solution (final concentration 0.77 mg/mL) was added to the mixture containing 3.5 µL of water, 5 µL of aqueous solution of diethylenetriaminepentaacetic acid (DTPA; final concentration 4 mM) and 1 µL of DEPMPO (final concentration 3.5 mM). Upon the addition of 7.5 µL of aqueous solution of riboflavin (final concentration 0.75 mM), the sample was irradiated with 30 W UV light during 30 s and

transferred into the gas-permeable Teflon tube. EPR spectra were recorded 2 min after the riboflavin addition using the following experimental settings: microwave power 10 mW, microwave frequency 9.85 GHz, modulation frequency 100 kHz, modulation amplitude 2 G, 5 accumulations. To assess the ability of GQD to quench NO radicals, the solution consisting of GQD, SNP as an NO radical-generating system, and $Fe(DTCS)_2$ complex as a spin-trapping agent was used [41,44]. In brief, 25 µl of sample which contained 19 µl of GQD solution (final concentration 0.63 mg/mL) and 6 µl of $Fe(DTCS)_2$ complex (final concentration 0.1 M) was transferred into the gas-permeable Teflon tube and 5 µl of SNP (final concentration 9 mM) was added just before the EPR spectra was acquired. The NO-$Fe(DTCS)_2$ spin-adduct EPR signal was measured using the following experimental settings: microwave power 10 mW, microwave frequency 9.85 GHz, modulation frequency 100 kHz, modulation amplitude 2 G. The control systems for all three radical types were made the same way as described above, but without GQD. To get the best insight into the amount of free-radicals which were present in the explored systems, all experimental EPR spectra were computer-simulated (Bruker SpinFit software) using simulation parameters indicated in [41]. The results obtained from the double-integration of simulated EPR spectra were used to calculate the quenching activity of GQD.

Cell culture

All reagents were purchased from Merck KgaA (Darmstadt, Germany), unless stated otherwise. The human neuroblastoma cell line SH-SY5Y (ATCC CRL-2266) was grown at 37°C in a humidified atmosphere with 5% CO_2, in a Modified Eagle Medium + F12 cell culture medium (1:1) supplemented with 10% fetal calf serum, L-glutamine (2 mM), nonessential amino acids, penicillin (100 IU/mL), and streptomycin (100 µg/mL). The trypsinized cells were incubated in 96-well flat-bottom cell culture plates (3×10^4 cells/well)

for the cell viability assessment, 24-well plates (3×10^5 cells/well) for the flow cytometric analysis, or 90 mm cell culture plates (7×10^6 cells) for the immunoblotting, malondialdehyde (MDA) assay, and electron microscopy. Cells were rested for 24 h and then treated with GQD and/or SNP in the presence or absence of caspase inhibitor Q-VD-Oph, NO scavenger 4,4,5,5-tetramethylimidazoline-1-oxyl 3-oxide (PTIO), $ONOO^-$ scavenger uric acid, iron chelators DTPA and 4,7-diphenyl-1,10-phenanthrolinedisulfonic acid (BPDSA), or autophagy inhibitors bafilomycin A_1, NH_4Cl, wortmannin, and 3-methyladenine. Alternatively, cells were treated with NO donor diethylamine NONOate (DEA-NONOate) instead of SNP, while GQD were replaced with antioxidants glutathione, N-acetylcysteine (NAC), dimethyl sulfoxide (DMSO), α-tocopherol, or superoxide dismutase (SOD). The incubation times and concentrations of agents are stated in figure legends and/or figures.

Cell viability assays

The staining of adherent cells with crystal violet and measurement of mitochondrial dehydrogenase-dependent reduction of 3-(4,5-dimethylthiazol-2-yl)-2, 5-diphenyltetrazolium bromide (MTT) to formazan were used to determine cell viability as previously described [45]. The cell viability was expressed as % of the control value (untreated cells), which was arbitrarily set to 100%, and the IC_{50} values were calculated using the Prism (version 8) software (GraphPad Software, San Diego, CA). Alternatively, dead cells were detected based on their permeability for the trypan blue stain. After the treatment, cells were collected by trypsinization, stained with 0.2% trypan blue solution, and both live (trypan $blue^-$) and dead (trypan $blue^+$) cells were counted using a hemocytometer.

Apoptosis analysis

Flow cytometry was used to assess nuclear DNA fragmentation and depolarization of mitochondrial membrane as markers of apoptotic cell death. For the DNA fragmentation analysis, cells were fixed in 70% ethanol at 4°C and incubated with RNAse (50 μg/mL) and DNA-binding dye propidium iodide (40 μg/mL) in PBS at 4°C overnight. The proportion of cells in different cell cycle phases, including hypodiploid apoptotic cells in sub-G_0/G_1 compartment, was determined by measuring the red fluorescence of propidium iodide on a FACSCalibur flow cytometer with CellQuest Pro software (BD Biosciences, Heidelberg, Germany), using FL2-W vs. FL2-A dot plot to exclude cell aggregates. The mitochondrial depolarization was assessed using JC-1 (5',6,6'-tetrachloro-1,1',3,3'-tetraethylbenzimidazolylcarbocyanine iodide), a lipophilic cation that forms orange-red fluorescent aggregates upon binding to a polarized mitochondrial membrane. If the mitochondrial membrane potential is disturbed, the dye cannot access the transmembrane space and remains or reverts to its green monomeric form. The cells were stained with JC-1 (2 μM) in cell culture medium at 37°C, 5% CO_2, for 15 min, washed and resuspended in PBS, and the green monomers and red aggregates were detected using FACSCalibur flow cytometer and CellQuest Pro software. The results are presented as the ratio between the green and red fluorescence of JC-1 (mean FL1/FL2), the increase of which reflects mitochondrial depolarization. The FL1/FL2 value in untreated control cells was arbitrarily set to 1.

TEM analysis of cellular morphology

For the analysis of ultrastructural morphology by TEM, trypsinized cells were fixed with 3% glutaraldehyde in cacodylate buffer and post-fixed in 1% osmium tetroxide. After dehydration in graded alcohols, cells were embedded in Epoxy medium. The ultra-thin

sections were stained with uranyl acetate and lead citrate for examination on a Morgagni 268D electron microscope (FEI, Hillsboro, OR). The images were acquired using a MegaView III CCD camera equipped with iTEM software (Olympus Soft Imaging Solutions, Münster, Germany).

Detection of intracellular acidic vesicles

The staining with a pH-sensitive dye acridine orange was used to determine intracellular acidification as a measure of number/volume of acidic vesicles (lysosomes and autolysosomes). After the treatment, cells were washed with PBS, stained with acridine orange (1 μM) for 15 min at 37ºC, trypsinized, and analyzed by flow cytometry using a FACSCalibur flow cytometer and CellQuest software. The acidic lysosomal content was quantified as the red/green fluorescence ratio (FL3/FL1), and the results were presented relative to the value obtained in untreated cells, which was arbitrarily set to 1.

Lipid peroxidation

Malondialdehyde, an indicator of lipid peroxidation, was measured using a colorimetric thiobarbituric acid assay. The binding of thiobarbituric acid to malondialdehyde-bis-(dimethylacetal)1,1,3,3-tetramethoxypropan, formed during lipid peroxidation, produces a chromogenic complex. The homogenate obtained by lysing the cells with 10% ice-cold trichloroacetic acid was centrifuged at 800 g for 10 min, and the supernatant was mixed (1:1) with 0.6% 2-thiobarbituric acid and heated in a boiling water for 10 min. The absorbance was measured at 535 nm using a microplate reader, and the results are expressed as the fold change of absorbance intensity relative to untreated cells.

Detection of intracellular and extracellular ROS and RNS

Intracellular ROS production was determined by measuring the fluorescence intensity emitted by a redox-sensitive dye dihydrorhodamine (DHR), while the production of RNS was measured using NO/$ONOO^-$-sensitive fluorochrome diaminofluorescein (DAF). Briefly, DHR (2 μM) was added at the beginning, whereas DAF (20 μM) was added during the last 30 min of treatment. After washing of cells in PBS, the mean intensity of green (FL1) fluorescence, corresponding to ROS/RNS production, was determined using a FACSCalibur flow cytometer and CellQuest software. Alternatively, DHR and DAF were used to determine ROS/RNS in the cell-free conditions, using Chameleon (Hidex, Turku, Finland) microplate fluorescence reader (excitation 488 nm, detection 535 nm). The intracellular levels of superoxide anion were measured by a modified version of a previously described assay for superoxide-dependent intracellular conversion of nitro blue tetrazolium (NBT) to formazan [46]. Briefly, after 15 min of incubation at 37°C with NBT (50 mM), cells were fixed in absolute ethanol and allowed to air dry. The cellular formazan was then solubilized with 1 mM NaOH in DMSO, and the absorbance was measured at 570 nm using a microplate reader. Intracellular $^{\bullet}OH$ levels were determined using a fluorometric Mitochondrial Hydroxyl Radical Detection Assay Kit (Abcam, Cambridge, UK), according to the manufacturer's instructions. Briefly, cells were incubated with OH580 probe for 1 h at 37°C before treatment. After washing with PBS, assay buffer was added to cells and red fluorescence signal (excitation 540 nm, detection 590 nm) was measured using a microplate fluorescence reader. Cellular production of NO was also determined by measuring the accumulation of NO end-product nitrite in the cell culture supernatants, using the Griess reagent. Briefly, 50 μl aliquots of cell culture supernatants were mixed with an equal volume of Griess reagent (mixture at 1:1 of 0.1% naphthylethylenediamine dihydrochloride and 1% sulfanilamide in 5% H_3PO_4) in a flat-bottom 96-well plate. After 10 min at room temperature,

the absorbance at 570 nm was measured using a microplate reader, and nitrite concentration was calculated from a $NaNO_2$ standard curve.

Immunoblot analysis

Cells were lysed in the lysis buffer (30 mM Tris-HCl pH 8.0, 150 mM NaCl, 1% NP-40 and protease/phosphatase inhibitor cocktail; all from KGaA, Darmstadt, Germany), stored on ice for 30 min, centrifuged at 14000 g for 15 minutes at 4°C, and the supernatants were collected. Equal protein amounts from each sample were separated by sodium dodecyl sulfate-polyacrylamide gel electrophoresis and transferred to nitrocellulose membranes (Bio-Rad, Hercules, CA). Rabbit anti-human antibodies against cleaved caspase-2 (#2224), poly (ADP-ribose) polymerase 1 (PARP1; #9542), microtubule-associated protein 1 light chain 3B (LC3B; #2775), mTOR (#2983), phospho-mTOR (Ser2448; #2971), Akt (#9272), phospho-Akt (Thr308; #4056), proline-rich Akt substrate of 40 kDa (PRAS40; #2610), phospho-PRAS40 (Thr246; #2640), actin (#4967) (all from Cell Signaling Technology, Beverly, MA), sequestosome-1/p62 (NBP1-48320), and beclin-1 (NB500-249) (both from Novus Biologicals, Littleton, CO) were used as primary antibodies. Peroxidase-conjugated goat anti-rabbit IgG (#7074, Cell Signaling Technology) was used as a secondary antibody, and the specific protein bands were visualized by enhanced chemiluminescence using ChemiDoc MP Imaging System (Bio-Rad, Hercules, CA). The intensity of protein bands was measured by densitometry using Image Lab software (Bio-Rad) and the obtained results were expressed relative to the intensity of total protein signals (for phosphorylated proteins) or actin (for cleaved caspase-2, cleaved PARP1, LC3-II, beclin-1, and p62).

Quantitative reverse transcription- polymerase chain reaction (RT-qPCR)

Total RNA was extracted using RNeasy Protect Mini Kit (Qiagen, Hilden, Germany), and the reverse transcription reaction was performed using MuLV reverse transcriptase and random hexamers (Thermo Fisher Scientific, Waltham, MA), according to the manufacturer's instructions. RT-qPCR was performed in a Realplex^2 Mastercycler (Eppendorf, Hamburg, Germany) using MicroAmp Optical 96-well reaction plates, TaqMan Universal PCR Master Mix, and TaqMan primers/probes (all from Thermo Fisher Scientific) for human ATF4 (Hs00909569_g1), ATG3 (Hs00223937_m1), ATG4B (Hs00367088_m1), ATG5 (Hs00169468_m1), ATG7 (Hs00197348_m1), ATG10 (Hs009197718_m1), ATG14 (Hs00208732_m1), BCL2 (Hs00608023_m1), BNIP3 (Hs00969291_m1), GABARAP (Hs00925899_g1), PIK3C3 (Hs00176908_m1), UVRAG (Hs01075434_m1), and the two housekeeping genes: TBP (Hs99999910_m1) and HPRT1 (Hs99999909_m1). The cycle of threshold (Ct) value of the geomean of the two housekeeping genes was subtracted from the Ct values of the target genes to obtain ΔCt values, and the ΔΔCt values were obtained by subtracting the ΔCt values of different treatments from the ΔCt values of the untreated control. The relative mRNA expression was determined as $2^{-\Delta\Delta Ct}$, and the results were presented as the fold change relative to the mRNA levels in the untreated control.

Statistical analysis

The statistical significance of the differences was analyzed by the t-test or one-way ANOVA followed by Tukey's test for multiple comparisons. A p value of less than 0.05 was considered statistically significant, and the compact letter display was used to label statistically significant differences (the same letter denotes no difference).

Results

Characterization of GQD

The optical, structural, and morphological properties of GQD used in the present study are presented in Figure 1. UV-Vis spectrum of GQD shows a band at 210 nm, which originates from $\pi \rightarrow \pi^*$ transition in the aromatic C-C bonds, as well as the shoulder band at around 345 nm that stems from $n \rightarrow \pi^*$ transition of C=O bonds (Fig. 1A). In the FTIR spectrum of GQD, bands from O-containing functional groups are detected at 1700, 1360, and 1010 cm^{-1}, corresponding to C=O, O=C-O, and C-O bonds, respectively (Fig. 1B). The bands from O-H bonds are detected in the 3100-3400 cm^{-1} range, while other bands stem from different C-C bonds (Fig. 1B). Both UV-Vis and FTIR spectra prove that GQD possess domains with aromatic C atoms, as well as O-containing functional groups. The photoluminescence spectra of GQD excited with the wavelengths from 300 to 400 nm are presented in Fig. 1C. The highest intensity of the emission was detected upon the excitation wavelength of 360 nm, with the center of emission at 465 nm. The blue emission of GQD above 450 nm has been attributed to electron-hole recombination or quantum size effect/zig-zag effect [47]. Different excitation wavelengths lead to the shifted center of the emission bands from 430 to 490 nm, which is common for GQD [48,49]. The morphology of GQD was investigated using both AFM and HR-TEM (Fig. 1D-F). AFM image shows that GQD were round-shaped and well dispersed, without observable agglomerates (Fig. 1D). The height of GQD varied from 1 to 12 nm, suggesting that they mostly contained several graphene layers. HR-TEM images revealed that GQD were 10-15 nm in diameter (Fig. 1E), with the lattice spacing of approx. 0.25 nm (Fig. 1F), which is close to the hexagonal pattern of graphene and consistent with previously reported findings [50].

Antioxidant activity of GQD in cell-free conditions

As antioxidant action is one of the hallmarks of GQD biological activity, we first examined the ability of the above described GQD to quench biologically relevant ROS/RNS in cell-free conditions. A general antioxidant capacity of GQD was demonstrated by the decoloration of the purple-colored free radical DPPH (Fig. 2A), and the reduction of SNP-induced fluorescence of the nonselective redox-sensitive dye DHR (Fig. 2B). GQD also decreased NBT oxidation by alkaline DMSO-derived superoxide (Fig. 2A), Fenton reaction-mediated generation of hydroxyl radical (Fig. 2A), and SNP-induced fluorescence of NO-selective fluorochrome DAF (Fig. 2B). The ability of GQD to quench $^{\bullet}OH$, $O_2^{\bullet-}$ and NO radicals was additionally confirmed by EPR analysis (Fig. 2C-E). For that purpose, normalized double integral values calculated from the computer simulation of experimental EPR spectra were used. The quenching activity (QA) of GQD was calculated using the formula:

$$QA = \frac{A_o - A_c}{A_o} 100\ (\%)$$

where Ao and Ac refer to the double integral values of computer-simulated EPR spectra without and with GQD, respectively. As it could be observed, GQD displayed a very high quenching activity towards $^{\bullet}OH$ (>99.3%), $O_2^{\bullet-}$ (91.5%) and NO radicals (84.4%).

GQD protect SH-SY5Y human neuroblastoma cells from SNP-induced toxicity

To test the neuroprotective potential of GQD, we assessed their effect on SNP-induced death of SH-SY5Y human neuroblastoma cells, which have been frequently used for the *in vitro* analysis of neurotoxicity/neuroprotection [12,14,51]. SH-SY5Y cells were treated with SNP

(0.5-2 mM) in the presence or absence of GQD (50-400 μg/mL) for 24 h, and the cell viability was assessed by measuring mitochondrial dehydrogenase activity (MTT test) and cell number (crystal violet staining). While SNP expectedly caused a dose-dependent cytotoxicity, the treatment with GQD restored the cell viability, as confirmed by both MTT and crystal violet test (Fig. 3A, B). The protective effect of GQD was concentration-dependent, particularly in the cells exposed to 1 mM and 2 mM SNP (Fig. 3A, B). Our preliminary experiments have shown that the toxicity of 1 mM SNP was largely exerted through an antiproliferative effect, while 2 mM SNP caused more overt cell death and was therefore chosen for further experiments. Light microscopy examination revealed that GQD alone had no discernible effect on the morphology of SH-SY5Y cells, but clearly prevented SNP-induced cell rounding and detachment from the surface of the cell culture well (Fig. 3C). The staining with trypan blue demonstrated that SNP increased the proportion of dead cells unable to exclude the dye, which was efficiently counteracted by GQD (Fig. 3D). The extensive washing of SH-SY5Y cells preincubated with GQD only partly reduced their protective activity (Fig. 3E), suggesting that the intracellular presence of GQD was required for optimal protection. Indeed, we observed a time-dependent increase in red fluorescence (FL3) of SH-SY5Y cells incubated with GQD, indicating their cellular internalization (Fig. 3F). While due to the small size of GQD it was difficult to observe the intracellular presence of single nanoparticles by TEM, their occasional aggregates were readily noticeable (Fig. 3G). Collectively, these data confirm the ability of GQD to enter SH-SY5Y cells and protect them from the toxicity of SNP.

GQD inhibit SNP-induced apoptotic death of SH-SY5Y cells

We next investigated the mechanisms responsible for the neuroprotective action of GQD. TEM analysis demonstrated that GQD prevented SNP-induced chromatin condensation and nuclear fragmentation as morphological characteristics of apoptotic cell death (Fig. 4A). Accordingly, cell cycle analysis of propidium iodide-stained cells showed that SNP-mediated increase in the percentage of cells with fragmented DNA (sub-G_0/G_1 compartment) was completely diminished by GQD (Fig. 4B). Moreover, immunoblot analysis revealed that GQD prevented SNP-induced cleavage/activation of DNA-repairing enzyme PARP1, as well as caspase-2 (Fig. 4C), an executioner caspase activated by oxidative stress and involved in permeabilization of the outer mitochondrial membrane [52]. The increase in green/red fluorescence ratio of JC-1, reflecting mitochondrial depolarization as another feature of apoptotic cells, was evident in SNP-treated cells, but markedly less so in the presence of GQD (Fig. 4D). In accordance with the above findings, pan-caspase inhibitor Q-VD-OPh rescued SH-SY5Y cells from SNP, thus confirming the pivotal role of caspase-dependent apoptosis in SNP-mediated cell death (Fig. 4E). Therefore, GQD suppress SNP-induced mitochondrial depolarization, caspase activation, and subsequent apoptotic demise of SH-SY5Y cells.

Quenching of NO and $^{\bullet}OH$ contributes to GQD-mediated protection from SNP toxicity

We next assessed the role of ROS/RNS scavenging in GQD-mediated protection from SNP. Consistent with the results obtained in cell-free conditions (Fig. 2B, E), flow cytometric analysis of cells stained with DAF, a florescent dye fairly selective for $NO/ONOO^-$, confirmed that GQD reduced RNS concentration in SNP-exposed SH-SY5Y cells (Fig. 5A).

Accordingly, the accumulation of the NO end-product nitrite in the supernatants of SNP-treated SH-SY5Y cells, measured by Griess reaction, was reduced by GQD to a certain extent (Fig. 5B). GQD also reduced nitrite accumulation in the supernatants of cells treated with another NO donor, DEA-NONOate (Fig. 5C), which was associated with partial recovery of cell viability (Fig. 5D). NO scavenger carboxy-PTIO and $ONOO^-$ scavenger uric acid marginally suppressed the neurotoxicity of SNP (Fig. 5E), and the "exhausted" SNP solution devoid of the ability to release NO by 72 h exposure to light [53] was only slightly less toxic to SH-SY5Y cells than fresh SNP (Fig. 5F). Moreover, GQD were still able to suppress this NO-independent toxicity of SNP (Fig. 5F), indicating that NO scavenging was involved in, but not crucial for the protective action of GQD in SNP-exposed SH-SY5Y cells. Again, in accordance with the data of cell-free measurements (Fig. 2A, B), NBT test and flow cytometric analysis of cells stained with ROS-sensitive dye DHR confirmed the ability of GQD to reduce SNP-mediated ROS increase in SH-SY5Y cells (Fig. 5G, H). Using a kit for selective detection of mitochondrial hydroxyl radical and MDA assay, we also demonstrated the ability of GQD to prevent SNP-induced intracellular $^{\bullet}OH$ accumulation (Fig. 5I) and lipid peroxidation (Fig. 5J), respectively. Iron chelators DTPA and BPDSA diminished the toxic effects of SNP against SH-SY5Y cells (Fig. 5K), implying that Fe^{2+} participated in SNP-mediated neurotoxicity. Finally, nonselective antioxidants glutathione and its precursor NAC, as well as relatively selective $^{\bullet}OH$ scavenger DMSO and lipid peroxidation inhibitor tocopherol-α mimicked the neuroprotective activity of GQD (Fig. 5L). Interestingly, superoxide dismutase (SOD) was not able to prevent and even potentiated SNP-induced cell death to a certain extent (Fig. 5L). Therefore, neutralization of $^{\bullet}OH$ formed in Fenton reaction catalyzed by SNP-derived iron, rather than $O_2^{\bullet-}$ quenching, was involved in GQD-mediated protection from SNP cytotoxicity.

GQD induce autophagy associated with reduced Akt/mTOR signaling in SNP-treated cells

While investigating the intracellular localization of GQD, we noticed that combined SNP/GQD treatment induced intracellular vacuolization of SH-SY5Y cells with the appearance of both double-membrane autophagosome-like and single-membrane autolysosome-like vesicles containing cellular material (Fig. 6A, black and white arrows, respectively). Immunoblot analysis demonstrated that both GQD and SNP alone only slightly increased the expression of proautophagic molecule beclin-1 and conversion of LC3-I into lipidated, autophagosome-associated form LC3-II, while reducing the levels of p62, the cargo receptor selectively degraded by autophagy (Fig. 6B). The autophagy-associated changes observed after single SNP or GQD administration were markedly more pronounced upon the combined treatment (Fig. 6B). Autophagy induction by SNP/GQD combination correlated with the inhibition of the main autophagy suppressor mTOR and its upstream activator Akt, as well as with the reduction of Akt-dependent phosphorylation of the mTOR-binding protein PRAS40 (Thr246) (Fig. 6C). The autophagy-inducing capacity of GQD, SNP, and particularly their combination, was further confirmed by the increase in intracellular acidification (Fig. 6D), which is consistent with the autophagy-associated accumulation of autolysosomes and lysosomes. RT-qPCR analysis revealed that GQD also increased the levels of mRNA encoding proautophagic molecules ATF4, ATG14, and ATG5, while simultaneously decreasing the mRNA levels of autophagy inhibitor BCL2 (Fig. 6E). SNP upregulated only ATG14 mRNA, while combined treatment further down-regulated BCL2 mRNA and increased the expression of ATF4 and ATG14 mRNA, as well as mRNA encoding autophagic activators ATG3 and ATG5 (Fig. 6E). Collectively, these data indicate that SNP and GQD synergize in inducing autophagy through both inhibition of Akt/mTOR signaling and transcriptional activation.

GQD-induced autophagy is cytoprotective independently of their antioxidant activity

While the increase in LC3-II levels resulting from its increased production reflects a genuine induction of autophagy, it could also be a consequence of reduced LC3-II degradation in autophagosomes, indicating a decrease in autophagic flux [54]. To clarify this issue, we assessed the autophagic flux by measuring the LC3-II levels in the presence of bafilomycin A1, a proton pump inhibitor that blocks autophagic proteolysis by inhibiting lysosomal acidification [55]. Both GQD and SNP alone, as well as their combination additionally up-regulated the levels of LC3-II in the presence of bafilomycin A1, thus confirming the increase in autophagosome formation and autophagic flux (Fig. 7A). In contrast to GQD, $^{\bullet}OH$ scavenger DMSO and antioxidant NAC failed to increase autophagic flux in combination with SNP (Fig. 7A, B), suggesting that the ability of GQD to induce autophagy in SNP-treated cells was independent of their antioxidant activity. Finally, to determine the role of autophagy in the cytoprotective action of GQD, we blocked the early phase of autophagy with the inhibitors of autophagosome formation wortmannin and 3-methyladenine, as well as the late, degradative stage of autophagy with NH_4Cl, an inhibitor of lysosomal acidification. While autophagy inhibitors did not significantly affect the viability of untreated cells or cells exposed to SNP or GQD alone, they markedly increased the cytotoxicity of the combined treatment (Fig. 7C). Therefore, GQD protect SNP-treated SH-SY5Y cells by stimulating prosurvival autophagy independently of their antioxidant activity.

Discussion

The present study for the first time demonstrates the ability of GQD to protect SH-SY5Y neuroblastoma cells from SNP-mediated oxidative/nitrosative stress by preventing

mitochondrial depolarization, caspase activation, and subsequent apoptotic cell death. GQD exerted the observed protection by quenching •OH, and to a lesser extent NO, as well as independently of their antioxidant activity through the induction of autophagy via Akt/mTOR suppression and transcriptional activation.

In accordance with the previously reported ROS- and NO-scavenging activity of GQD [24,27,56,57], we used EPR, chemical radical scavenging assays, and cytofluorometry to confirm their ability to neutralize •OH, $O_2^{\bullet-}$, and NO in cell-free conditions, as well as in SNP-treated SH-SY5Y cells. Somewhat surprisingly, the cytotoxicity of SNP in our experiments was mostly independent of NO, which was only marginally involved in the protection from SNP-induced cells death. This was indicated by the rather weak protective effect of NO scavengers, almost unaltered toxicity of SNP after exhausting its NO-generating capacity by light exposure, and the efficient GQD-mediated protection from exhausted SNP. These results are consistent with those of Cardaci et al., who found that the toxicity of SNP towards SH-SY5Y cells was independent of released NO and actually mediated by iron-catalyzed ROS generation [14]. Accordingly, SNP-released iron was found to trigger the production of highly cytotoxic •OH via Fenton reaction in both biological systems [13,58] and cell-free conditions [53]. In line with these findings, the reduction of SNP cytotoxicity by iron chelators and different antioxidants confirmed the pivotal role of Fenton reaction in our experimental system. In contrast, extracellularly applied SOD stimulated SNP neurotoxicity, which is consistent with its ability to decompose $O_2^{\bullet-}$ into O_2 and H_2O_2, leading to the formation of •OH in the Fenton reaction [53]. Moreover, mitochondrial hydroxyl radical detection assay and the reduction of SNP toxicity by the •OH scavenger DMSO indicate that the protective action of GQD could be at least partly attributed to •OH quenching. This was further supported by GQD-mediated decrease in SNP-triggered lipid peroxidation, which is

mainly induced by •OH and HOO• [59], as well as by mimicking GQD protective effect by lipid peroxidation inhibitor tocopherol-α.

The above discussed findings clearly indicate the role of •OH, and to a lower degree, NO neutralization in the cytoprotective activity of GQD, but there is a question if these effects were exerted intracellularly or extracellularly. Both possibilities seem plausible, as chondrocyte apoptosis depended on extracellular Fenton reaction between SNP-derived iron ions and H_2O_2 [53], while SNP internalization was required for the toxicity towards PC12 pheochromocytoma cell line and rat hepatocytes [60,61]. Accordingly, we have employed various approaches to demonstrate •OH, $O_2^{\bullet-}$, and NO quenching by GQD both in cell-free systems and SNP-treated SH-SY5Y cells. Although the flow cytometry analysis of SNP-exposed cells argues in favor of the intracellular antioxidant activity of GQD, the observed decrease of cellular ROS/RNS could also results from their extracellular scavenging and subsequent decrease in cell entry. However, this might be likely for the relatively long-lived NO, $O_2^{\bullet-}$ and H_2O_2, which could survive long enough to diffuse a few tens of micrometers, but markedly less so for the extremely reactive, short-lived •OH [62,63]. On the other hand, it is possible that GQD could decrease the extracellular levels of SNP-derived $O_2^{\bullet-}$ and H_2O_2, thus reducing their intracellular turnover into •OH. Nevertheless, a line of evidence in addition to cytofluorometric assays supports the involvement of intracellular antioxidant activity of GQD in their cytoprotective action. Namely, in accordance with previous results obtained by us and others in various cell types *in vitro* and *in vivo* [19-23], the TEM analysis and the increase in cellular fluorescence confirmed that GQD were internalized by SH-SY5Y cells. Moreover, the removal of GQD from extracellular space only partly diminished their prosurvival effect, indicating its dependence on the intracellular accumulation of GQD.

Importantly, the present study for the first time demonstrates the role of autophagy in GQD-mediated protection from oxidative/nitrosative stress. Following the recent guidelines [54], we used a multifaceted approach to confirm the ability of GQD to potentiate autophagic response in SNP-treated SH-SY5Y cells. Accordingly, we observed the increase in intracellular acidification, TEM-verified presence of autophagic vesicles, expression of proautophagic beclin-1, autophagy-selective degradation of p62, and LC3-I conversion to autophagosome-associated LC3-II in the presence of lysosomal inhibition, reflecting a genuine increase in autophagic turnover (flux) in GQD+SNP-treated cells. While confirming previously reported autophagy-inducing capacity of both GQD [21,28,29] and SNP [30-32], our study demonstrate their synergistic proautophagic action in SH-SY5Y cells. This cooperation was apparently exerted both at the signaling and transcriptional level, leading to inhibition of Akt/PRAS40/mTOR pathway and increased expression of several ATG genes. As Akt-dependent phosphorylation of PRAS40 at Thr246 is known to activate mTOR-containing autophagy repressor mTOR complex 1 (mTORC1) [64], it is plausible that Akt inhibition-mediated decrease in PRAS40 phosphorylation caused mTORC1 suppression and subsequent autophagy induction in GQD/SNP-exposed cells. Accordingly, it has been proposed that nanoparticles might interfere with mTOR activity either by preventing its localization to lysosomes or by affecting recruitment/activation of cell membrane-localized Akt during cellular internalization [65]. The transcriptional activation of autophagy by GQD or its combination with SNP involved the expression of autophagy transcription factor ATF4 [66], as well as ATG14, ATG5, and ATG3, which sequentially participate in autophagosome nucleation, autophagosome elongation, and LC3 lipidation leading to autophagosome closure, respectively [67]. Interestingly, the mRNA levels of BCL2, which inhibits autophagy by binding beclin-1, the crucial member of autophagy-initiating complex [67], were reduced by GQD, thus presumably further contributing to their autophagy-inducing action.

The pharmacological inhibition of either early (autophagosome formation) or late (lysosomal degradation) stages of autophagy revealed its crucial role in GQD-mediated protection from SNP. On the other hand, autophagy inhibition failed to affect the cytotoxicity of SNP alone, which also increased autophagic flux, albeit to a lower extent. This could be explained by the possibility that autophagy must exceed a certain threshold to become cytoprotective, as well by the findings that autophagy induced by different stimuli could differently affect the viability of the same cell type [68,69]. Although antioxidants have been shown to induce autophagy in certain conditions [70-72], they failed to mimic autophagy-potentiating effect of GQD in SNP-treated cells, indicating the independence of prosurvival autophagy on GQD antioxidant action. However, it is possible that a reverse interaction might occur, in which autophagy affects the antioxidant function of GQD. Namely, it has been demonstrated in various experimental models that autophagy suppresses oxidative stress-induced apoptotic death of SH-SY5Y cells by participating in the clearance of damaged mitochondria [73,74]. As the damaged mitochondria themselves release excessive amounts of ROS [75], this implies an interesting possibility that autophagy/mitophagy induction by GQD might contribute to their antioxidant activity. This assumption is currently being tested in our laboratory.

The main limitations of the present study include the in vitro experimental setting and the use of a rather high concentration of GQD (400 μg/mL), which is unlikely to be attained in vivo. However, it should be noted that at less toxic SNP doses GQD were protective at the concentration as low as 50 μg/mL. Moreover, GQD seem to penetrate the damaged blood-brain barrier more easily, thus presumably leading to enhanced local accumulation in the affected brain tissue [19]. Finally, GQD might be chemically modified for increased ROS-quenching and/or autophagy-inducing capacity [29,76], which might enable the

cytoprotective action at lower concentrations. Regardless of whether our findings could be translated to an in vivo setting, they nevertheless indicate that autophagy-inducing antioxidants may provide increased neuroprotection from oxidative/nitrosative stress.

In conclusion, our study demonstrates that •OH/NO quenching and Akt/mTOR-dependent autophagy induction independently cooperate in GQD-mediated protection of SH-SY5Y neuronal cells from SNP-induced apoptotic death. While these findings remain to be confirmed in primary neurons and *in vivo*, the unique capacity of GQD to act both as antioxidants and inducers of prosurvival autophagy, coupled with low toxicity and the ability to cross blood-brain barrier [27,77] qualifies them as potential candidates for the treatment of oxidative/nitrosative stress-associated neurodegenerative and neuroinflammatory disorders.

Acknowledgements

This study was supported by the Ministry of Education, Science and Technological Development of the Republic of Serbia (Contract No. 451-03-9/2021-14/200007, 451-03-9/2021-14/200110, 451-03-9/2021-14/200017, 451-03-9/2021-14/200026, and 451-03-9/2021-14/200146). The authors thank Dragan Bešević and Miloš Kiš (Institute of Histology and Embryology, Faculty of Medicine, University of Belgrade) for the technical assistance with TEM.

References

[1] S. Di Meo, T.T. Reed, P. Venditti, V.M. Victor, Role of ROS and RNS sources in physiological and pathological conditions, Oxid. Med. Cell. Longev. 2016 (2016) 1245049. doi: 10.1155/2016/1245049

[2] K.H. Lee, M. Cha, B.H. Lee, Neuroprotective effect of antioxidants in the brain, Int. J. Mol. Sci. 21 (2020). doi: 10.3390/ijms21197152

[3] P.S. Garry, M. Ezra, M.J. Rowland, J. Westbrook, K.T. Pattinson, The role of the nitric oxide pathway in brain injury and its treatment - from bench to bedside, Exp. Neurol. 263 (2015) 235-243. doi: 10.1016/j.expneurol.2014.10.017

[4] X. Wang, E.K. Michaelis, Selective neuronal vulnerability to oxidative stress in the brain, Front. Aging Neurosci. 2 (2010) 12. doi: 10.3389/fnagi.2010.00012

[5] R.M. Berg, K. Moller, D.M. Bailey, Neuro-oxidative-nitrosative stress in sepsis, J. Cereb. Blood Flow Metab. 31 (2011) 1532-1544. doi: 10.1038/jcbfm.2011.48

[6] A. Phaniendra, D.B. Jestadi, L. Periyasamy, Free radicals: properties, sources, targets, and their implication in various diseases, Indian J. Clin. Biochem. 30 (2015) 11-26. doi: 10.1007/s12291-014-0446-0

[7] A.R. Butler, I.L. Megson, Non-heme iron nitrosyls in biology, Chem. Rev. 102 (2002) 1155-1166. doi: 10.1021/cr000076d

[8] Y.Y. Quan, Y.H. Liu, C.M. Lin, X.P. Wang, T.S. Chen, Peroxynitrite dominates sodium nitroprusside-induced apoptosis in human hepatocellular carcinoma cells, Oncotarget 8 (2017) 29833-29845. doi: 10.18632/oncotarget.16164

[9] M. Jang, E.J. Cho, X.L. Piao, Protective effects of resveratrol oligomers from Vitis amurensis against sodium nitroprusside-induced neurotoxicity in human neuroblastoma SH-SY5Y cells, Arch. Pharm. Res. 38 (2015) 1263-1269. doi: 10.1007/s12272-014-0505-3

[10] H.S. Chun, W.C. Low, Ursodeoxycholic acid suppresses mitochondria-dependent programmed cell death induced by sodium nitroprusside in SH-SY5Y cells, Toxicology 292 (2012) 105-112. doi: 10.1016/j.tox.2011.11.020

[11] M.S. Kim, J. Lee, H.S. So, K.M. Lee, B.S. Moon, H.S. Lee, R. Park, Danchunhwan water extract prevents apoptotic death by peroxynitrite and nitric oxide in human dopaminergic neuroblastoma SH-SY5Y cells, Immunopharmacol. Immunotoxicol. 23 (2001) 239-252. doi: 10.1081/iph-100103863

[12] W. Kamoshima, Y. Kitamura, Y. Nomura, T. Taniguchi, Possible involvement of ADP-ribosylation of particular enzymes in cell death induced by nitric oxide donors in human neuroblastoma cells, Neurochem. Int. 30 (1997) 305-311. doi: 10.1081/iph-100103863

[13] P. Rauhala, A. Khaldi, K.P. Mohanakumar, C.C. Chiueh, Apparent role of hydroxyl radicals in oxidative brain injury induced by sodium nitroprusside, Free Radic. Biol. Med. 24 (1998) 1065-1073. doi: 10.1016/s0891-5849(97)00386-9

[14] S. Cardaci, G. Filomeni, G. Rotilio, M.R. Ciriolo, Reactive oxygen species mediate p53 activation and apoptosis induced by sodium nitroprusside in SH-SY5Y cells, Mol. Pharmacol. 74 (2008) 1234-1245. doi: 10.1124/mol.108.048975

[15] V. Weissig, D. Guzman-Villanueva, Nanocarrier-based antioxidant therapy: promise or delusion?, Expert Opin. Drug Deliv. 12 (2015) 1783-1790. doi: 10.1517/17425247.2015.1063611

[16] T. Gao, X. Wang, L.Y. Yang, H. He, X.X. Ba, J. Zhao, F.L. Jiang, Y. Liu, Red, yellow, and blue luminescence by graphene quantum dots: syntheses, mechanism, and cellular imaging, ACS Appl. Mater. Interfaces 9 (2017) 24846-24856. doi: 10.1021/acsami.7b05569

[17] L. Nilewski, K. Mendoza, A.S. Jalilov, V. Berka, G. Wu, W.K.A. Sikkema, A. Metzger, R. Ye, R. Zhang, D.X. Luong, T. Wang, E. McHugh, P.J. Derry, E.L. Samuel, T.A.

Kent, A.L. Tsai, J.M. Tour, Highly oxidized graphene quantum dots from coal as efficient antioxidants, ACS Appl. Mater. Interfaces 11 (2019) 16815-16821. doi: 10.1021/acsami.9b01082

[18] Y.C. Shi, J.J. Feng, S.S. Chen, G.M. Tu, J.R. Chen, A.J. Wang, Simple synthesis of hierarchical AuPt alloy nanochains for construction of highly sensitive hydrazine and nitrite sensors, Mater. Sci. Eng. C Mater. Biol. Appl. 75 (2017) 1317-1325. doi: 10.1016/j.msec.2017.03.041

[19] J. Tosic, Z. Stanojevic, S. Vidicevic, A. Isakovic, D. Ciric, T. Martinovic, T. Kravic-Stevovic, V. Bumbasirevic, V. Paunovic, S. Jovanovic, B. Todorovic-Markovic, Z. Markovic, M. Danko, M. Micusik, Z. Spitalsky, V. Trajkovic, Graphene quantum dots inhibit T cell-mediated neuroinflammation in rats, Neuropharmacology 146 (2019) 95-108. doi: 10.1016/j.neuropharm.2018.11.030

[20] V. Volarevic, V. Paunovic, Z. Markovic, B. Simovic Markovic, M. Misirkic-Marjanovic, B. Todorovic-Markovic, S. Bojic, L. Vucicevic, S. Jovanovic, N. Arsenijevic, I. Holclajtner-Antunovic, M. Milosavljevic, M. Dramicanin, T. Kravic-Stevovic, D. Ciric, M.L. Lukic, V. Trajkovic, Large graphene quantum dots alleviate immune-mediated liver damage, ACS Nano 8 (2014) 12098-12109. doi: 10.1021/nn502466z

[21] Z.M. Markovic, B.Z. Ristic, K.M. Arsikin, D.G. Klisic, L.M. Harhaji-Trajkovic, B.M. Todorovic-Markovic, D.P. Kepic, T.K. Kravic-Stevovic, S.P. Jovanovic, M.M. Milenkovic, D.D. Milivojevic, V.Z. Bumbasirevic, M.D. Dramicanin, V.S. Trajkovic, Graphene quantum dots as autophagy-inducing photodynamic agents, Biomaterials 33 (2012) 7084-7092. doi: 10.1016/j.biomaterials.2012.06.060

[22] L. Xu, Y. Dai, Z. Wang, J. Zhao, F. Li, J.C. White, B. Xing, Graphene quantum dots in alveolar macrophage: uptake-exocytosis, accumulation in nuclei, nuclear responses and DNA cleavage, Part. Fibre Toxicol. 15 (2018) 45. doi: 10.1186/s12989-018-0279-8

[23] X.Y. Wang, R. Lei, H.D. Huang, N. Wang, L. Yuan, R.Y. Xiao, L.D. Bai, X. Li, L.M. Li, X.D. Yang, The permeability and transport mechanism of graphene quantum dots (GQDs) across the biological barrier, Nanoscale 7 (2015) 2034-2041. doi: 10.1039/c4nr04136d

[24] Y. Chong, C. Ge, G. Fang, X. Tian, X. Ma, T. Wen, W.G. Wamer, C. Chen, Z. Chai, J.J. Yin, Crossover between anti- and pro-oxidant activities of graphene quantum dots in the absence or presence of light, ACS Nano 10 (2016) 8690-8699. doi: 10.1021/acsnano.6b04061

[25] Z.M. Markovic, S.P. Jovanovic, P.Z. Maskovic, M.M. Mojsin, M.J. Stevanovic, M. Danko, M. Micusik, D.J. Jovanovic, A. Kleinova, Z. Spitalsky, V.B. Pavlovic, B.M. Todorovic Markovic, Graphene oxide size and structure pro-oxidant and antioxidant activity and photoinduced cytotoxicity relation on three cancer cell lines, J. Photochem. Photobiol. B 200 (2019) 111647. doi: 10.1016/j.jphotobiol.2019.111647

[26] B.Z. Ristic, M.M. Milenkovic, I.R. Dakic, B.M. Todorovic-Markovic, M.S. Milosavljevic, M.D. Budimir, V.G. Paunovic, M.D. Dramicanin, Z.M. Markovic, V.S. Trajkovic, Photodynamic antibacterial effect of graphene quantum dots, Biomaterials 35 (2014) 4428-4435. doi: 10.1016/j.biomaterials.2014.02.014

[27] K. Tak, R. Sharma, V. Dave, S. Jain, S. Sharma, Clitoria ternatea mediated synthesis of graphene quantum dots for the treatment of alzheimer's disease, ACS Chem. Neurosci. 11 (2020) 3741-3748. doi: 10.1021/acschemneuro.0c00273

[28] S. Tomić, K. Janjetović, D. Mihajlović, M. Milenković, T. Kravić-Stevović, Z. Marković, B. Todorović-Marković, Z. Spitalsky, M. Micusik, D. Vučević, M. Čolić, V.

Trajković, Graphene quantum dots suppress proinflammatory T cell responses via autophagy-dependent induction of tolerogenic dendritic cells, Biomaterials 146 (2017) 13-28. doi: 10.1016/j.biomaterials.2017.08.040

[29] Y. Xie, B. Wan, Y. Yang, X. Cui, Y. Xin, L.H. Guo, Cytotoxicity and autophagy induction by graphene quantum dots with different functional groups, J. Environ. Sci. (China) 77 (2019) 198-209. doi: 10.1016/j.jes.2018.07.014

[30] S.Y. Park, M.Y. Park, H.G. Park, K.J. Lee, M.S. Kook, W.J. Kim, J.Y. Jung, Nitric oxide-induced autophagy and the activation of activated protein kinase pathway protect against apoptosis in human dental pulp cells, Int. Endod. J. 50 (2017) 260-270. doi: 10.1111/iej.12616

[31] J.Y. Yang, M.Y. Park, S.Y. Park, H.I. Yoo, M.S. Kim, J.H. Kim, W.J. Kim, J.Y. Jung, Nitric oxide-induced autophagy in MC3T3-E1 cells is associated with cytoprotection via AMPK activation, Korean J. Physiol. Pharmacol. 19 (2015) 507-514. doi: 10.4196/kjpp.2015.19.6.507

[32] L. Zang, H. He, Y. Ye, W. Liu, S. Fan, S. Tashiro, S. Onodera, T. Ikejima, Nitric oxide augments oridonin-induced efferocytosis by human histocytic lymphoma U937 cells via autophagy and the NF-κB-COX-2-IL-1β pathway, Free Radic. Res. 46 (2012) 1207-1219. doi: 10.3109/10715762.2012.700515

[33] I. Dikic, Z. Elazar, Mechanism and medical implications of mammalian autophagy, Nat. Rev. Mol. Cell Biol. 19 (2018) 349-364. doi: 10.1038/s41580-018-0003-4

[34] F.M. Menzies, K. Moreau, D.C. Rubinsztein, Protein misfolding disorders and macroautophagy, Curr. Opin. Cell Biol. 23 (2011) 190-197. doi: 10.1016/j.ceb.2010.10.010

[35] C. Fang, L. Gu, D. Smerin, S. Mao, X. Xiong, The interrelation between reactive oxygen species and autophagy in neurological disorders, Oxid. Med. Cell. Longev. 2017 (2017) 8495160. doi: 10.1155/2017/8495160

[36] H.T. Li, X.D. He, Z.H. Kang, H. Huang, Y. Liu, J.L. Liu, S.Y. Lian, C.H.A. Tsang, X.B. Yang, S.T. Lee, Water-soluble fluorescent carbon quantum dots and photocatalyst design, Angew. Chem. Int. Edit. 49 (2010) 4430-4434. doi: 10.1002/anie.200906154

[37] S. Jovanović, S. Dorontić, D. Jovanović, G. Ciasca, M. Budimir, A. Bonasera, M. Scopelliti, O. Marković, B. Todorović Marković, Gamma irradiation of graphene quantum dots with ethylenediamine: Antioxidant for ion sensing, Ceram Int 46 (2020) 23611-23622. doi: https://doi.org/10.1016/j.ceramint.2020.06.133

[38] N. Smirnoff, Q.J. Cumbes, Hydroxyl radical scavenging activity of compatible solutes, Phytochemistry 28 (1989) 1057-1060. doi: https://doi.org/10.1016/0031-9422(89)80182-7

[39] E. Kunchandy, M.N.A. Rao, Oxygen radical scavenging activity of curcumin, Int. J. Pharm. 58 (1990) 237-240. doi: https://doi.org/10.1016/0378-5173(90)90201-E

[40] S.K. Jackson, K.J. Liu, M. Liu, G.S. Timmins, Detection and removal of contaminating hydroxylamines from the spin trap DEPMPO, and re-evaluation of its use to indicate nitrone radical cation formation and S_N1 reactions, Free Radic. Biol. Med. 32 (2002) 228-232. doi: 10.1016/s0891-5849(01)00795-x

[41] Đ. Nakarada, B. Pejin, G. Tommonaro, M. Mojović, Liposomal integration method for assessing antioxidative activity of water insoluble compounds towards biologically relevant free radicals: example of avarol, J. Liposome Res. 30 (2020) 218-226. doi: 10.1080/08982104.2019.1625378

[42] A.G. Savić, M. Mojović, Free radicals identification from the complex EPR signals by applying higher order statistics, Anal. Chem. 84 (2012) 3398-3402. doi: 10.1021/ac300200y

[43] F.A. Villamena, C.M. Hadad, J.L. Zweier, Kinetic study and theoretical analysis of hydroxyl radical trapping and spin adduct decay of alkoxycarbonyl and dialkoxyphosphoryl nitrones in aqueous media, J Phys. Chem. A 107 (2003) 4407-4414. doi: 10.1021/jp027829f

[44] B.V. Stefánsson, A.L. Björnson, B. Haraldsson, U.A. Nilsson, A new method for monitoring nitric oxide production using Teflon membrane microdialysis, Free Radic. Biol. Med. 39 (2005) 249-256. doi: 10.1016/j.freeradbiomed.2005.03.019

[45] M. Kosic, K. Arsikin-Csordas, V. Paunovic, R.A. Firestone, B. Ristic, A. Mircic, S. Petricevic, M. Bosnjak, N. Zogovic, M. Mandic, V. Bumbasirevic, V. Trajkovic, L. Harhaji-Trajkovic, Synergistic anticancer action of lysosomal membrane permeabilization and glycolysis inhibition, J. Biol. Chem. 291 (2016) 22936-22948. doi: 10.1074/jbc.M116.752113

[46] A.S. Vrablic, C.D. Albright, C.N. Craciunescu, R.I. Salganik, S.H. Zeisel, Altered mitochondrial function and overgeneration of reactive oxygen species precede the induction of apoptosis by 1-O-octadecyl-2-methyl-rac-glycero-3-phosphocholine in p53-defective hepatocytes, FASEB J. 15 (2001) 1739-1744. doi: 10.1096/fj.00-0300com

[47] S. Zhu, J. Zhang, S. Tang, C. Qiao, L. Wang, H. Wang, X. Liu, B. Li, Y. Li, W. Yu, X. Wang, H. Sun, B. Yang, Surface chemistry routes to modulate the photoluminescence of graphene quantum dots: from fluorescence mechanism to up-conversion bioimaging applications, Adv. Funct. Mater. 22 (2012) 4732-4740. doi: https://doi.org/10.1002/adfm.201201499

[48] H. Ding, S.B. Yu, J.S. Wei, H.M. Xiong, Full-color light-emitting carbon dots with a surface-state-controlled luminescence mechanism, ACS Nano 10 (2016) 484-491. doi: 10.1021/acsnano.5b05406

[49] S.P. Jovanović, Z. Syrgiannis, M.D. Budimir, D.D. Milivojević, D.J. Jovanovic, V.B. Pavlović, J.M. Papan, M. Bartenwerfer, M.M. Mojsin, M.J. Stevanović, B.M. Todorović Marković, Graphene quantum dots as singlet oxygen producer or radical quencher - the matter of functionalization with urea/thiourea, Mater. Sci. Eng. C Mater. Biol. Appl. 109 (2020) 110539. doi: https://doi.org/10.1016/j.msec.2019.110539

[50] L. Song, J. Shi, J. Lu, C. Lu, Structure observation of graphene quantum dots by single-layered formation in layered confinement space, Chem. Sci. 6 (2015) 4846-4850. doi: 10.1039/C5SC01416F

[51] M. Tajes, G. Ill-Raga, E. Palomer, E. Ramos-Fernández, F.X. Guix, M. Bosch-Morató, et al., Nitro-oxidative stress after neuronal ischemia induces protein nitrotyrosination and cell death, Oxid. Med. Cell. Longev. 2013 (2013) 826143. doi: 10.1155/2013/826143

[52] L. Bouchier-Hayes, The role of caspase-2 in stress-induced apoptosis, J. Cell. Mol. Med. 14 (2010) 1212-1224. doi: 10.1111/j.1582-4934.2010.01037.x

[53] Y.Y. Quan, G.Q. Qin, H. Huang, Y.H. Liu, X.P. Wang, T.S. Chen, Dominant roles of Fenton reaction in sodium nitroprusside-induced chondrocyte apoptosis, Free Radic. Biol. Med. 94 (2016) 135-144. doi: 10.1016/j.freeradbiomed.2016.02.026

[54] D.J. Klionsky, A.K. Abdel-Aziz, S. Abdelfatah, M. Abdellatif, A. Abdoli, S. Abel, et al., Guidelines for the use and interpretation of assays for monitoring autophagy (4th edition), Autophagy 17 (2021) 1-382. doi: 10.1080/15548627.2020.1797280

[55] C. Mauvezin, T.P. Neufeld, Bafilomycin A1 disrupts autophagic flux by inhibiting both V-ATPase-dependent acidification and Ca-P60A/SERCA-dependent autophagosome-

lysosome fusion, Autophagy 11 (2015) 1437-1438. doi: 10.1080/15548627.2015.1066957

[56] Y. Xie, S. Yu, Y. Zhong, Q. Zhang, Y. Zhou, SnO_2/graphene quantum dots composited photocatalyst for efficient nitric oxide oxidation under visible light, Appl. Surf. Sci. 448 (2018) 655-661. doi: https://doi.org/10.1016/j.apsusc.2018.04.145

[57] A. Sun, L. Mu, X. Hu, Graphene oxide quantum dots as novel nanozymes for alcohol intoxication, ACS Appl. Mater. Interfaces 9 (2017) 12241-12252. doi: 10.1021/acsami.7b00306

[58] D.N. Ramakrishna Rao, A.I. Cederbaum, Generation of reactive oxygen species by the redox cycling of nitroprusside, Biochim. Biophys. Acta 1289 (1996) 195-202. doi: 10.1016/0304-4165(95)00158-1

[59] A. Ayala, M.F. Munoz, S. Arguelles, Lipid peroxidation: production, metabolism, and signaling mechanisms of malondialdehyde and 4-hydroxy-2-nonenal, Oxid. Med. Cell. Longev. 2014 (2014) 360438. doi: 10.1155/2014/360438

[60] D. Terwel, L.J. Nieland, B. Schutte, C.P. Reutelingsperger, F.C. Ramaekers, H.W. Steinbusch, S-nitroso-N-acetylpenicillamine and nitroprusside induce apoptosis in a neuronal cell line by the production of different reactive molecules, Eur. J. Pharmacol. 400 (2000) 19-33. doi: 10.1016/s0014-2999(00)00379-4

[61] D.N. Rao, S. Elguindi, P.J. O'Brien, Reductive metabolism of nitroprusside in rat hepatocytes and human erythrocytes, Arch. Biochem. Biophys. 286 (1991) 30-37. doi: 10.1016/0003-9861(91)90005-4

[62] D.D. Thomas, X. Liu, S.P. Kantrow, J.R. Lancaster, Jr., The biological lifetime of nitric oxide: implications for the perivascular dynamics of NO and O_2, Proc. Natl. Acad. Sci. USA 98 (2001) 355-360. doi: 10.1073/pnas.011379598

[63] F. Collin, Chemical basis of reactive oxygen species reactivity and involvement in neurodegenerative diseases, Int. J. Mol. Sci. 20 (2019). doi: 10.3390/ijms20102407

[64] Y. Sancak, C.C. Thoreen, T.R. Peterson, R.A. Lindquist, S.A. Kang, E. Spooner, S.A. Carr, D.M. Sabatini, PRAS40 is an insulin-regulated inhibitor of the mTORC1 protein kinase, Mol. Cell 25 (2007) 903-915. doi: 10.1016/j.molcel.2007.03.003

[65] L. Hulea, Z. Markovic, I. Topisirovic, T. Simmet, V. Trajkovic, Biomedical potential of mtor modulation by nanoparticles, Trends Biotechnol. 34 (2016) 349-353. doi: 10.1016/j.tibtech.2016.01.005

[66] W. B'Chir, A.C. Maurin, V. Carraro, J. Averous, C. Jousse, Y. Muranishi, L. Parry, G. Stepien, P. Fafournoux, A. Bruhat, The eIF2α/ATF4 pathway is essential for stress-induced autophagy gene expression, Nucleic Acids Res. 41 (2013) 7683-7699. doi: 10.1093/nar/gkt563

[67] J. Füllgrabe, D.J. Klionsky, B. Joseph, The return of the nucleus: transcriptional and epigenetic control of autophagy, Nat. Rev. Mol. Cell Biol. 15 (2014) 65-74. doi: 10.1038/nrm3716

[68] M. Bosnjak, B. Ristic, K. Arsikin, A. Mircic, V. Suzin-Zivkovic, V. Perovic, A. Bogdanovic, V. Paunovic, I. Markovic, V. Bumbasirevic, V. Trajkovic, L. Harhaji-Trajkovic, Inhibition of mTOR-dependent autophagy sensitizes leukemic cells to cytarabine-induced apoptotic death, PLoS One 9 (2014) e94374. doi: 10.1371/journal.pone.0094374

[69] B. Ristic, M. Bosnjak, K. Arsikin, A. Mircic, V. Suzin-Zivkovic, A. Bogdanovic, V. Perovic, T. Martinovic, T. Kravic-Stevovic, V. Bumbasirevic, V. Trajkovic, L. Harhaji-Trajkovic, Idarubicin induces mTOR-dependent cytotoxic autophagy in leukemic cells, Exp. Cell Res. 326 (2014) 90-102. doi: 10.1016/j.yexcr.2014.05.021

[70] J. Cui, L. Tang, Q. Hong, S. Lin, X. Sun, G. Cai, X.Y. Bai, X. Chen, N-acetylcysteine ameliorates gentamicin-induced nephrotoxicity by enhancing autophagy and reducing oxidative damage in miniature pigs, Shock 52 (2019) 622-630. doi: 10.1097/shk.0000000000001319

[71] Y. Yu, L. Hou, H. Song, P. Xu, Y. Sun, K. Wu, Akt/AMPK/mTOR pathway was involved in the autophagy induced by vitamin E succinate in human gastric cancer SGC-7901 cells, Mol. Cell. Biochem. 424 (2017) 173-183. doi: 10.1007/s11010-016-2853-4

[72] Y.M. Song, S.O. Song, Y.K. Jung, E.S. Kang, B.S. Cha, H.C. Lee, B.W. Lee, Dimethyl sulfoxide reduces hepatocellular lipid accumulation through autophagy induction, Autophagy 8 (2012) 1085-1097. doi: 10.4161/auto.20260

[73] A. Di Rita, P. D'Acunzo, L. Simula, S. Campello, F. Strappazzon, F. Cecconi, AMBRA1-mediated mitophagy counteracts oxidative stress and apoptosis induced by neurotoxicity in human neuroblastoma SH-SY5Y Cells, Front. Cell. Neurosci. 12 (2018) 92. doi: 10.3389/fncel.2018.00092

[74] H.T. Zhang, L. Mi, T. Wang, L. Yuan, X.H. Li, L.S. Dong, P. Zhao, J.L. Fu, B.Y. Yao, Z.C. Zhou, PINK1/Parkin-mediated mitophagy play a protective role in manganese induced apoptosis in SH-SY5Y cells, Toxicol. In Vitro 34 (2016) 212-219. doi: 10.1016/j.tiv.2016.04.006

[75] J. Dan Dunn, L.A. Alvarez, X. Zhang, T. Soldati, Reactive oxygen species and mitochondria: a nexus of cellular homeostasis, Redox Biol. 6 (2015) 472-485. doi: 10.1016/j.redox.2015.09.005

[76] Y. Wang, W. Kong, L. Wang, J.Z. Zhang, Y. Li, X. Liu, Y. Li, Optimizing oxygen functional groups in graphene quantum dots for improved antioxidant mechanism, Phys. Chem. Chem. Phys. 21 (2019) 1336-1343. doi: 10.1039/c8cp06768f

[77] T.K. Henna, K. Pramod, Graphene quantum dots redefine nanobiomedicine, Mater. Sci. Eng. C Mater. Biol. Appl. 110 (2020) 110651. doi: 10.1016/j.msec.2020.110651

Figure legends

Fig. 1. Characterization of GQD. The representative UV-Vis (A), FTIR (B), and photoluminescence (C) spectra, as well as AFM (D), TEM (E), and HRTEM (F) images are shown (a.u., arbitrary units).

Fig. 2. Antioxidant activity of GQD in cell-free conditions. (A, B) GQD (100 - 400 µg/mL) were incubated in cell-free conditions with stable DPPH radical, superoxide-generating alkaline DMSO, $^{\bullet}OH$-generating system (Fe^{2+}+ ascorbate + H_2O_2) (A), SNP (2 mM) + DHR (2 µM), or SNP + DAF (20 µM) (B). The absorbance of visible light at 517 nm or 570 nm, corresponding to DPPH, $O_2^{\bullet-}$, or $^{\bullet}OH$ levels (A), or the green fluorescence of DHR and DAF, as a measure of total ROS and NO production, respectively (B), was determined after 1 h (A) or 30 min (B). The data are mean ± SD values of triplicates from a representative of three experiments (A) or mean ± SD values from three independent experiments (B). (C-E) Alternatively, the ability of GQD (400 µg/mL) to scavenge $O_2^{\bullet-}$ (C), $^{\bullet}OH$ (D), and NO (E) was measured by EPR. The representative EPR spectra of DEPMPO/OH (C), DEPMPO/OOH (D) and NO-$Fe(DTCS)_2$ (E) spin-adducts without (control) and with GQD, recorded 2 min upon their generation, are shown.

Fig. 3. GQD protect SH-SY5Y cells from SNP-induced toxicity. (A-D) SH-SY5Y cells were incubated for 24 h with different concentrations (A, B) or 2 mM (C, D) of SNP in the

presence or absence of the indicated concentrations (A, B) or 400 μg/mL of GQD (C, D). Cell viability was assessed by MTT (A) and crystal violet assay (B), cell morphology was assessed by light microscopy (C), and the proportion of dead cells was determined by trypan blue staining (D). (E) After 1 h incubation with GQD (400 μg/mL), SH-SY5Y cells were extensively washed with PBS and treated with SNP (2 mM) for an additional 24 h. Cell viability was determined by MTT test. (F, G) SH-SY5Y cells were incubated for the indicated time periods (F) or 24 h (G) with GQD (400 μg/mL), and their intracellular accumulation was assessed by flow cytometry (E) or TEM (F). The data are mean ± SD values of triplicates from a representative of three experiments (A, B, D, E) or mean ± SD values from three independent experiments (F). Representative micrographs from two independent experiments are shown in (C) and (G).

Fig. 4. GQD inhibit SNP-induced apoptotic death of SH-SY5Y cells. (A-E) SH-SY5Y cells were incubated with SNP (2 mM) in the presence or absence of GQD (400 μg/mL) (A-D) or Q-VD-OPH (10 μM) (E). After 24 h, cell ultrastructural morphology was visualized by TEM (A), DNA fragmentation was assessed by flow cytometric analysis of propidium iodide-stained cells (B), while cell viability was assessed using MTT assay (E). PARP1 cleavage and caspase-2 activity were analyzed by immunoblotting after 12 h (C), while mitochondrial depolarization was determined by flow cytometric analysis of JC1-stained cells after 6 h of treatment (D). Representative electron micrographs from two independent experiments (A), as well as representative histograms (B, D) and blots (C) from three independent experiments are shown. The data are mean ± SD values from three independent experiments (B, D) or mean ± SD values of triplicates from a representative of three experiments (E).

Fig. 5. (A-L) SH-SY5Y cells were treated with 2 mM of SNP (A, B, E-L), NO donor DEA-NONOate (C, D), or light-exhausted SNP (SNPex; F) in the presence or absence of 400 μg/mL (A, E-L) or indicated concentrations of GQD (B-D), NO scavenger PTIO (5 μM) or $ONOO^-$ scavenger uric acid (5 μM) (E), iron chelators DTPA (5 μM) or BPDSA (50 μM) (K), or antioxidants DMSO (0.5%), α-tocopherol (α-toc, 100 μM), glutathione (GSH, 100 μM), NAC (10 mM), and SOD (250 μg/mL) (L). After 6 h of incubation, intracellular concentration of NO in diaminofluorescein (DAF)-stained cells (A) and ROS in dihydrorhodamine (DHR)-stained cells (H) were measured by flow cytometry, while intracellular $^{\bullet}OH$ levels were determined by fluorimetry using Mitochondrial hydroxyl radical detection assay Kit (I). After 24 h of incubation, nitrite accumulation, cell viability, intracellular ROS generation, and lipid peroxidation were assessed by Griess reaction (B, C), MTT test (D-F, K, L), NBT assay (G), and MDA test (J), respectively. Representative flow citometry histograms from three independent experiments are shown (A, H). The data are presented as mean ± SD values of triplicates from a representative of three independent experiments (B-G, I-L).

Fig. 6. GQD induce autophagy associated with reduced Akt/mTOR signaling in SNP-treated cells. (A-E) SH-SY5Y cells were incubated with SNP (2 mM) and/or GQD (400 μg/mL) for 2 h (C, E) or 6 h (A, B, D). Intracellular morphology was visualized by electron microscopy (black arrow indicates single-membrane autophagosome-like vesicle; white arrows indicate double-membrane autolysosome-like vesicle) (A). The levels of autophagy markers (B) and activation of Akt/mTOR signaling axis (C) were determined by immunoblotting, intracellular acidification was estimated by flow cytometry in acridine orange (AO)-stained cells (D), and the expression of autophagy genes was analyzed by RT-qPCR (E). Representative micrographs (A) and blots (B, C) from three independent experiments are shown, while the

data in (B-E) are presented as mean ± SD values from three independent experiments (B-D) or triplicates from a representative of three experiments (E).

Fig. 7. GQD-induced autophagy is cytoprotective and independent of their antioxidant activity. (A-C) SH-SY5Y cells were incubated for 6 h with 2 mM SNP and 400 μg/mL GQD (A, C), 0.5% DMSO (A), or 10 mM NAC (B), in the presence or absence of 10 nM bafilomycin A1 (BAF), and the levels of LC3-II were analyzed by immunoblotting. Representative blots are shown, and the densitometry data are presented as mean ± SD values from three independent experiments. (C) SH-SY5Y cells were incubated for 24 h with 2 mM SNP and 400 μg/mL GQD, in the presence or absence of wortmannin (200 nM), NH_4Cl (25 mM) or 3-methyladenine (5 mM). Cell viability was assessed by MTT test, and the data are presented as triplicates from a representative of three experiments.

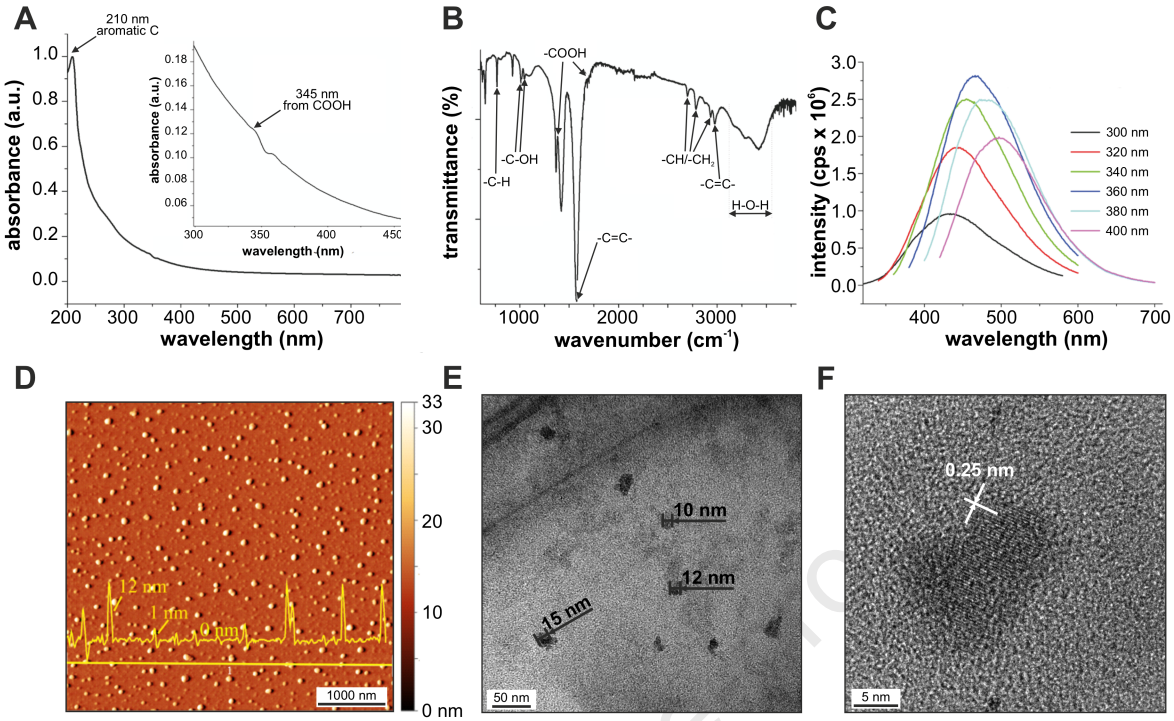

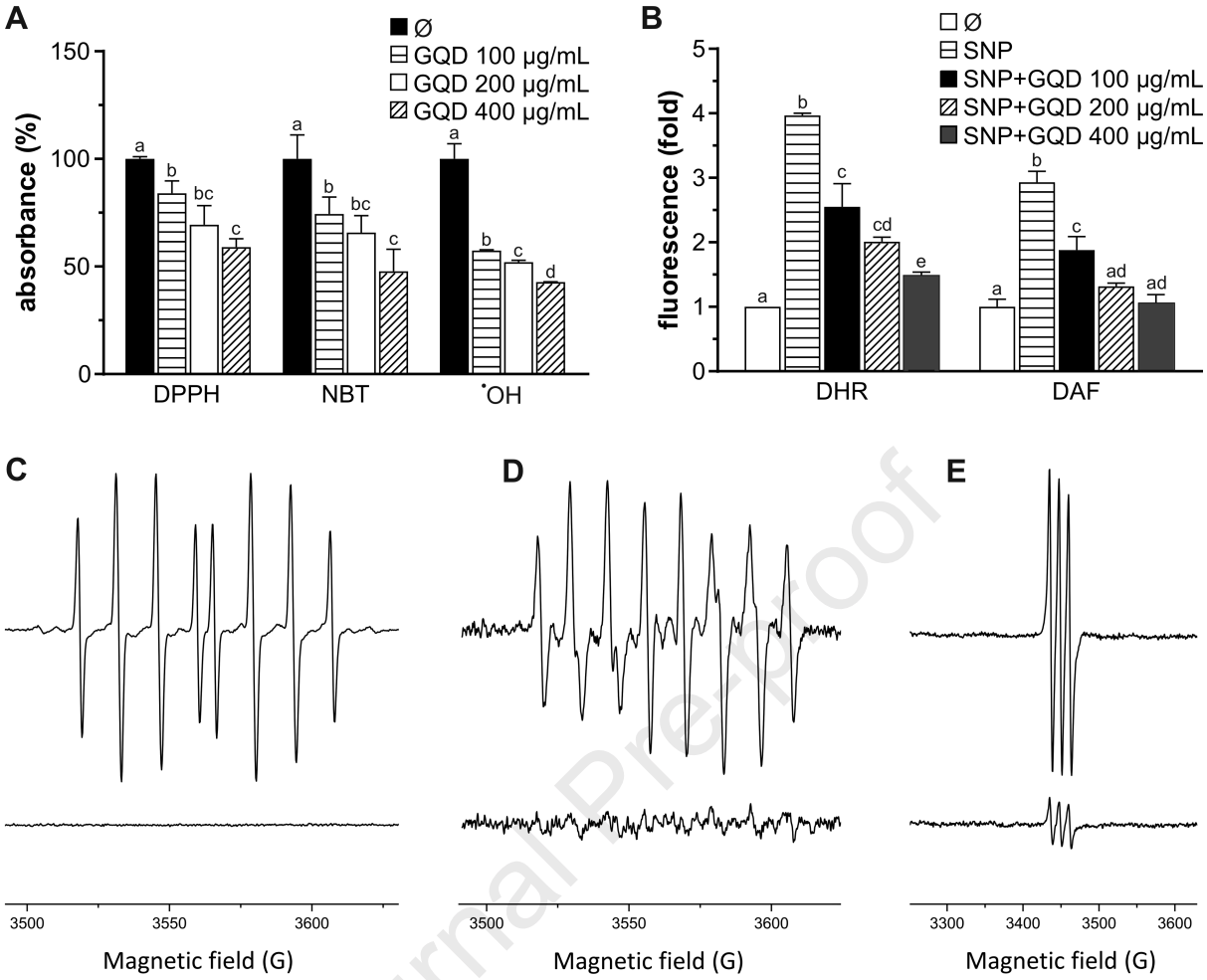

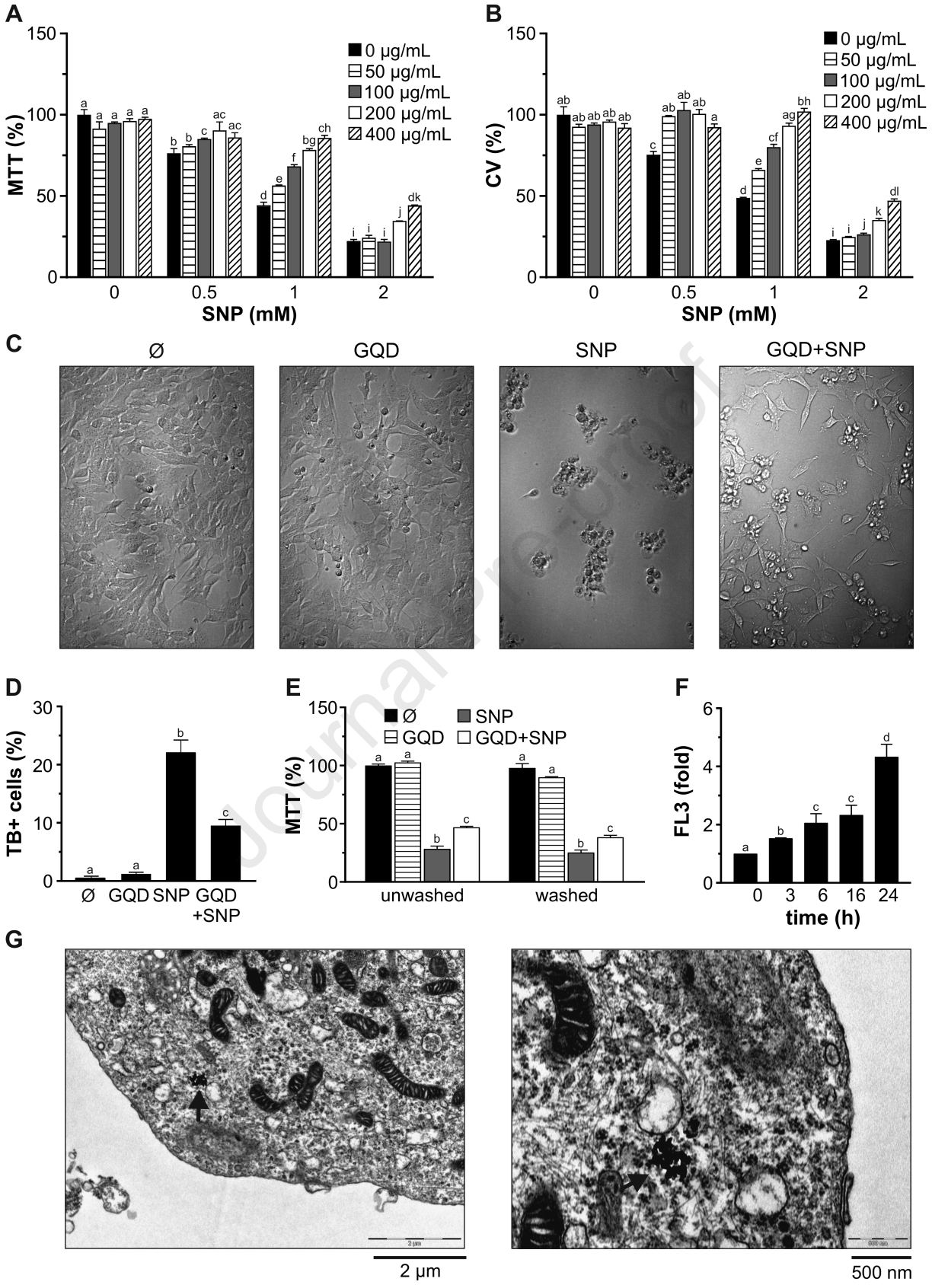

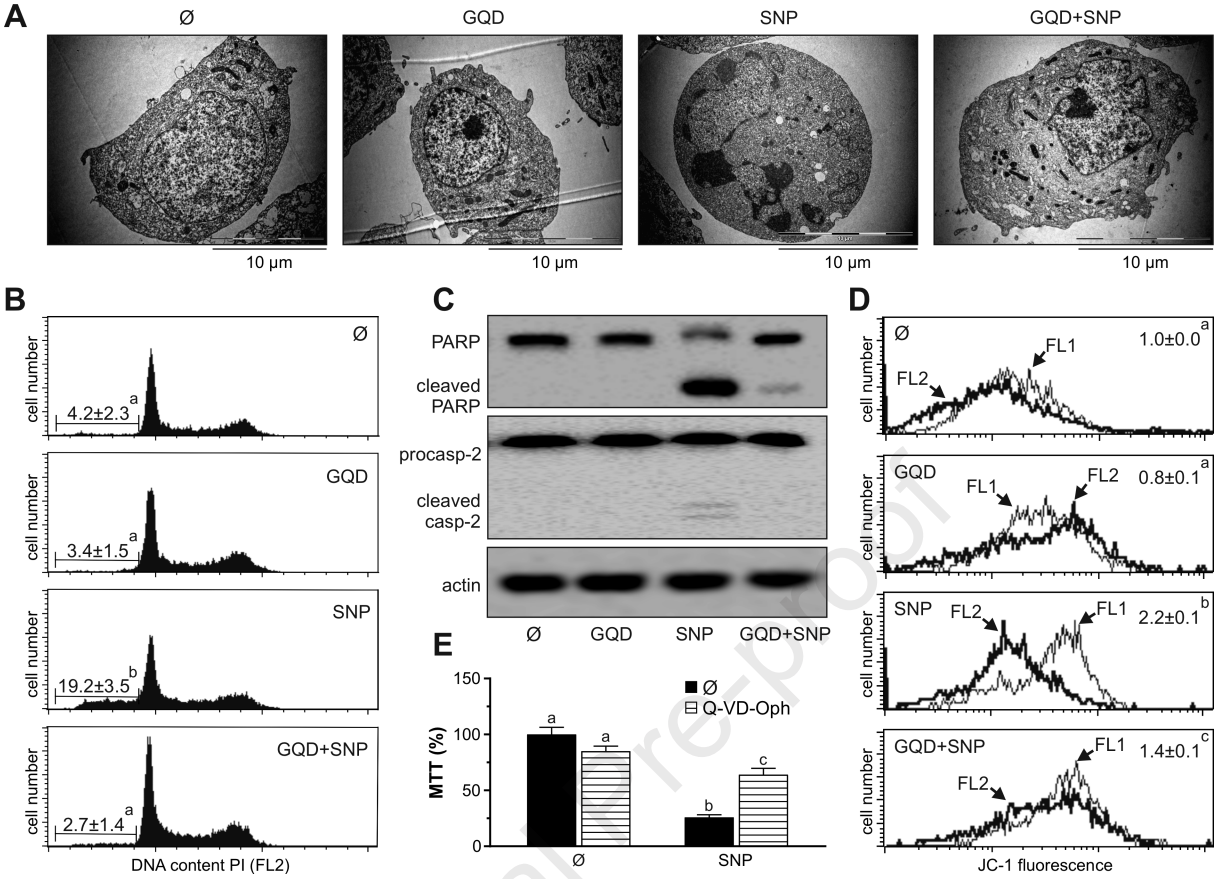

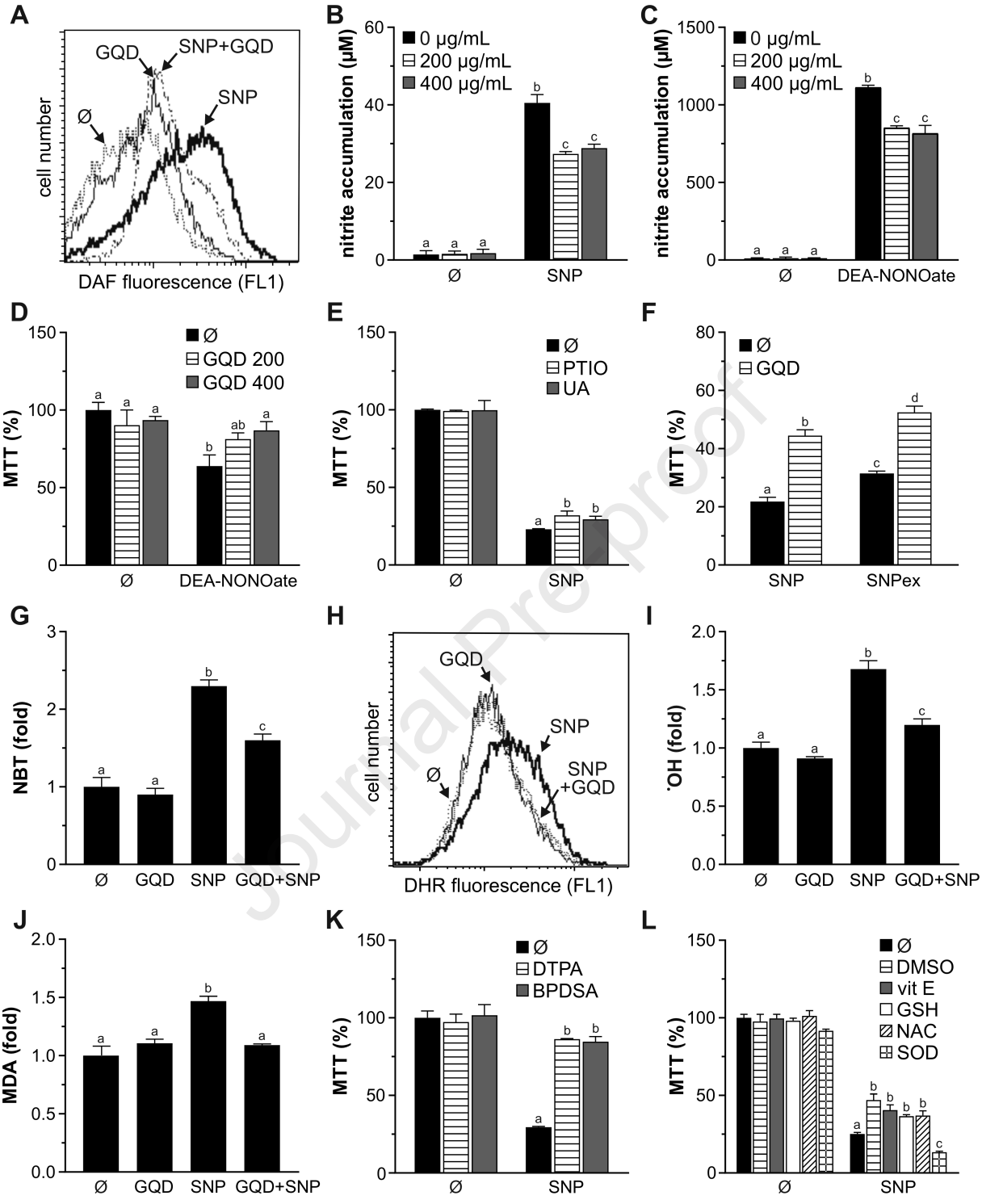
A
GQD
SNP+GQD
SNP
Ø
cell number
DAF fluorescence (FL1)
B
0 μg/mL
200 μg/mL
400 μg/mL
nitrite accumulation (μM)
Ø
SNP
C
0 μg/mL
200 μg/mL
400 μg/mL
nitrite accumulation (μM)
Ø
DEA-NONOate
D
Ø
GQD 200
GQD 400
MTT (%)
Ø
DEA-NONOate
E
Ø
PTIO
UA
MTT (%)
Ø
SNP
F
Ø
GQD
MTT (%)
SNP
SNPex
G
NBT (fold)
Ø
GQD
SNP
GQD+SNP
H
GQD
SNP
Ø
SNP +GQD
cell number
DHR fluorescence (FL1)
I
·OH (fold)
Ø
GQD
SNP
GQD+SNP
J
MDA (fold)
Ø
GQD
SNP
GQD+SNP
K
Ø
DTPA
BPDSA
MTT (%)
Ø
SNP
L
Ø
DMSO
vit E
GSH
NAC
SOD
MTT (%)
Ø
SNP

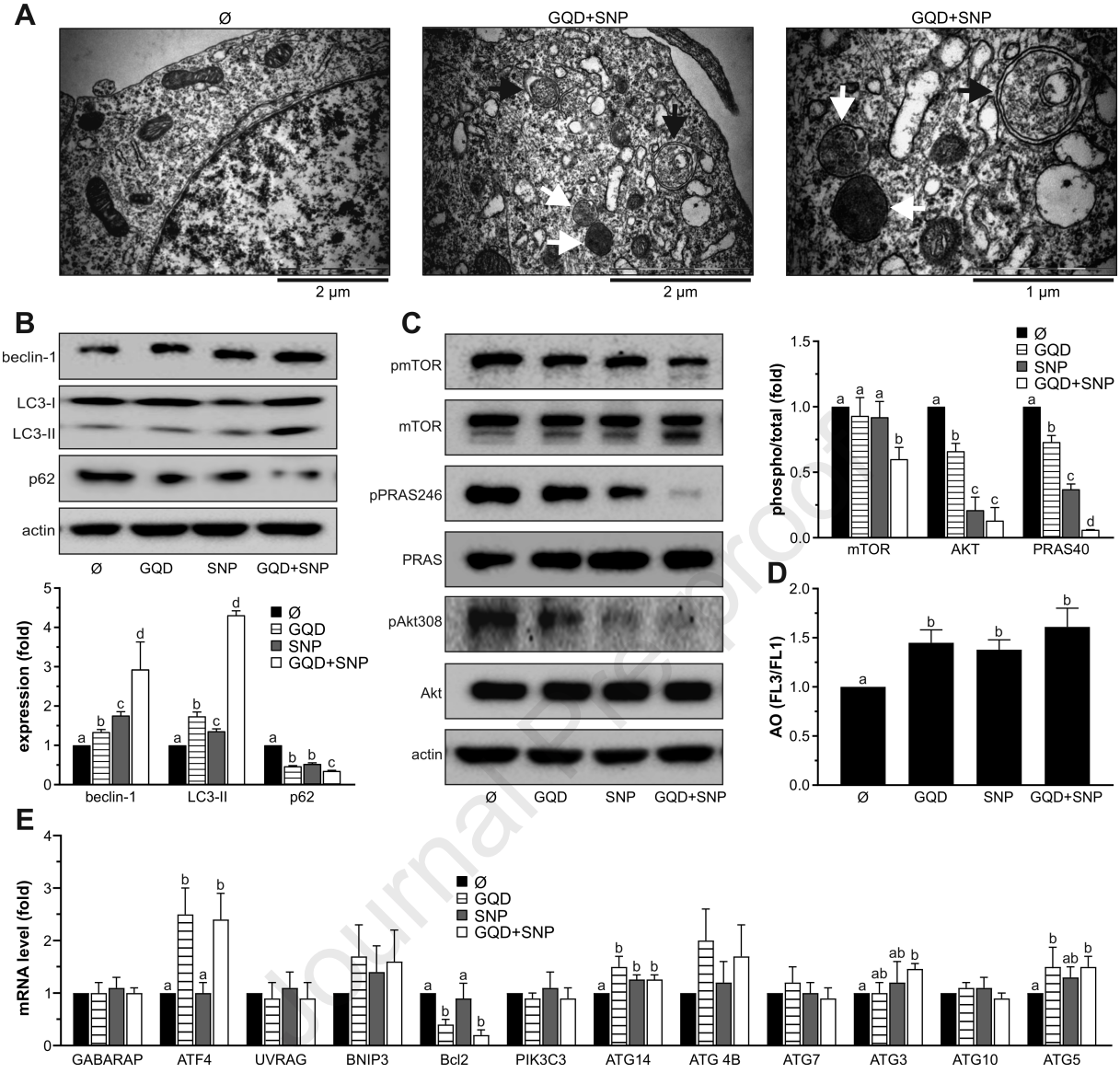

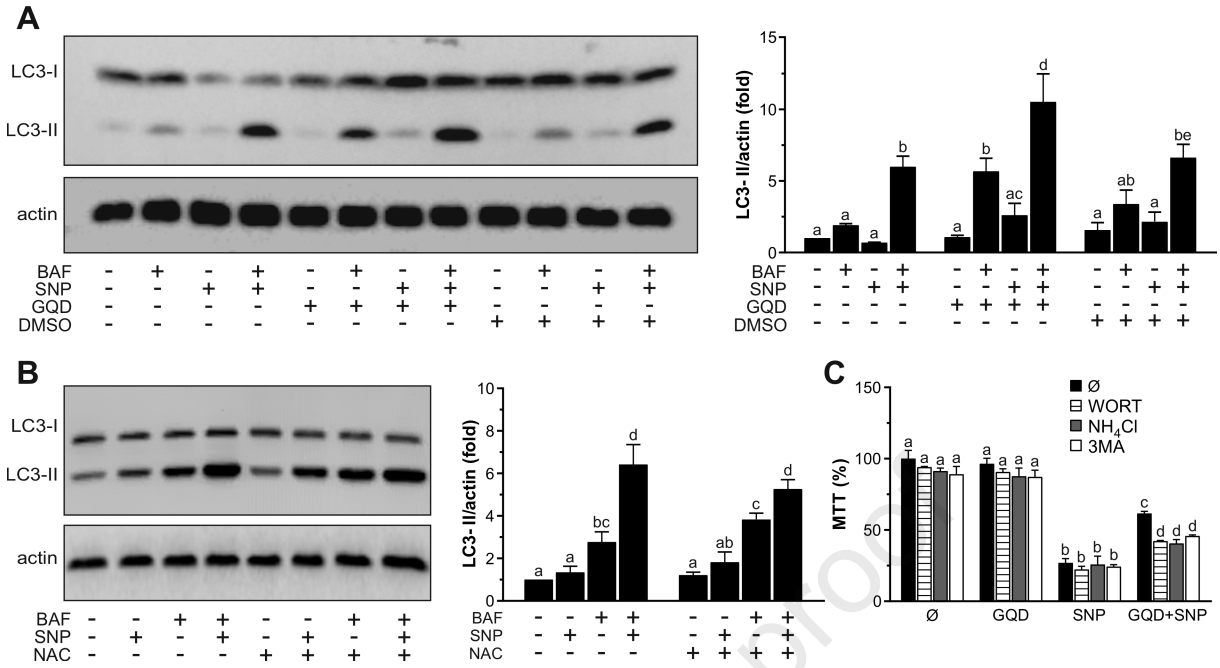

- Graphene quantum dots (GQD) protect SH-SY5Y cells from sodium nitroprusside (SNP)
- GQD inhibit SNP-induced apoptotic death of SH-SY5Y neuronal cells
- Quenching of NO and $^{\bullet}OH$ contributes to GQD-mediated protection from SNP toxicity
- GQD induce autophagy associated with reduced Akt/mTOR signaling
- GQD-induced autophagy is cytoprotective independently of their antioxidant activity